Journal of
GEOPHYSICAL RESEARCH

VOLUME 74 NOVEMBER 15, 1969 No. 25

Fine Structure of the Upper Mantle[1]

C. B. ARCHAMBEAU

Seismological Laboratory, California Institute of Technology
Pasadena, California 91109

E. A. FLINN AND D. G. LAMBERT

Seismic Data Laboratory, Teledyne Industries
Alexandria, Virginia 22304

The spectral amplitudes and travel times of seismic body waves are used to determine mantle velocity structures appropriate to distinct structural provinces within the western continental United States. In addition to basic amplitude and time data, travel-time delays and P_n velocity data from other studies are used as constraints in the systematic inversion of the data for mantle structure. The regional structures for the upper mantle determined in this manner show collectively rather sharp zones of transition (high velocity gradients) near 150, 400, 650 km and possibly near 1000 km. Comparatively, the regional structures indicate strong lateral variations in the upper mantle structure down to 150 km and possibly as deep as 200 km. The structures appropriate to the Rocky Mountain and Colorado plateau physiographic provinces show low-velocity zones capped by high-velocity lid zones, with variability in both the lid and the low-velocity zone properties from province to province and within these provinces to a much lesser degree. The mantle properties obtained for the Basin and Range contrast sharply with the plateau and mountain structures, with the lid zone being very thin or absent and abnormally low velocities extending from, or very near, the base of a thin crust to 150 km. The velocity determinations are coupled with estimates of the variation of the intrinsic dissipation function (Q) as a function of depth and frequency. These results show a pronounced low-Q zone corresponding to the average low-velocity zone depth range for the velocity models. The data suggest a frequency-dependent Q, with Q increasing with frequency. In total the results of the study strongly suggest phase transitions in the mantle, including a partially melted region corresponding to the low-velocity zone, the latter being highly variable in its properties over the region studied and strongly correlated with tectonic activity.

INTRODUCTION

A number of important geophysical questions about the internal structure and tectonic evolution of the earth can be answered only after we have obtained a more precise description of both the lateral and the radial variations of the properties of the earth's crust and mantle. Considerable knowledge of the spatial variations of the earth's continental crust is already available [for reviews, see *Brune*, 1969; *Steinhart and Meyer*, 1961; *Pakiser and Robinson*, 1966]. It is certain, however, that before a clear understanding of crustal structure and

[1] Contribution 1589, Division of Geological Sciences, California Institute of Technology.

crust-mantle processes is possible, similar information for the upper mantle will be required. In this study we have therefore attempted to determine the upper mantle structures that underlie particular continental provinces.

Toksöz and Anderson [1966] obtained several regional mantle models from studies of surface wave dispersion, corresponding to 'super provinces' designated as oceanic, tectonic, and shield structures. These models specify the shear-wave velocity as a function of depth. They probably represent averages of the actual mantle structure; for example, for the oceans, averages of mid-ocean ridge and ocean basin mantle structures, and, for the tectonic super province, averages of basin and range, plateau, and mountain structures. The models for shield areas [*Brune and Dorman*, 1963; *Barr*, 1967] and those for the plains area [*Lewis and Meyer*, 1968; *Green and Hales*, 1968] appear to be representative of essentially a single structural province.

In the present study we have obtained compressional velocity models appropriate for the tectonic region of the North American continent. We distinguish two basic types of mantle structure for a tectonic region: first, a basin and range or rift zone mantle structure and, second, a plateau-mountain structure. The desirability of further subdivision of these general structural types appears likely as more data become available, and the results of this study suggest that the plateau region we have examined may have an intermediate type of mantle structure that is midway in its properties between the Basin and Range and the mountain structures.

Among the objectives of this effort is the description of the properties of a continental block in sufficient detail to enable us to infer the dynamical processes that are taking place and that have taken place within the mantle underlying shields and stable regions as well as within tectonic regions on the borders of the continents. There are therefore a number of specific questions that concern us here. In particular, how does the upper mantle structure vary from one physiographic province to the next, and how is it correlated with these provinces and their boundaries, as well as with the surface geological and crustal properties? Is there a well-defined low-velocity zone for the compressional-wave velocity? If so, is the thickness of the crust and variation of velocity within the crust related to the variability of this zone in the upper mantle? If the presence of such a zone implies anomalously high temperatures, should we not expect that this would be reflected in the physical properties of the crust, if not in the surface geology as well? Is the nature of the low compressional-wave velocity zone in the upper mantle (where it occurs) such that it is indicative of partial melting? For, if the rate of change of velocity with depth is large both at the top and at the bottom edges of the zone, a conclusion supporting partial melting is difficult to escape. Further, is there a zone of high attenuation of seismic waves coincident in depth with the zone of low velocity, and are these zones correlated in their lateral variability? Is the low-velocity zone (where it exists) similarly correlated with heat flow, gravity, and other geophysical parameters? If it can be established that such correlations and relationships exist, then it is reasonable to hypothesize that at least certain kinds of tectonic activity are associated with the presence of a partially melted upper mantle. If these regions are also spatially associated with oceanic ridge systems, we will probably be in a position to understand more fully oceanic tectonics, as hypothesized by *Vine and Matthews* [1963] and discussed by *Isacks et al.* [1968], especially with regard to the connection between sea-floor spreading and continental tectonics.

Previous investigations of upper mantle velocity structure using surface wave dispersion (by *Anderson and Toksöz* [1963], in particular) have suggested velocity transition zones in the mantle. Studies using P-wave travel times and amplitudes by *Archambeau et al.* [1966, 1967], *Archambeau* [1966], *Lewis and Meyer* [1968], and *Green and Hales* [1968], as well as studies of apparent surface velocities of P waves ($dT/d\Delta$), such as those of *Niazi and Anderson* [1965], *Johnson* [1967], and *Kanamori* [1967*a*], have all arrived at velocity models that have rapid velocity increases in the ranges around 375 to 450 km and again from 650 to 700 km. *Anderson* [1967*a*], *Fujisawa* [1968], and *Akimoto and Fujisawa* [1968] have summarized some of the implications of these rapid velocity variations in terms of composition and solid-

solid phase changes at these depths. We have already noted the importance of any rapid velocity variations at the top and bottom of the mantle's low-velocity zone in terms of implications about solid-liquid phase changes. Therefore, in view of the importance of seismic observations in the determination of the state and chemical composition of the earth's mantle, a precise determination of the radial variation of elastic and anelastic properties, where effects due to lateral variations are minimized within a given province, are clearly of critical importance. In particular, we wish to determine the depths and velocity gradients for the rapid transition zones, as well as the over-all increases or decreases in velocity across them. From such measurements a more confident determination of mantle composition will follow. Again it is important to ascertain the variability of these zones from one mantle province to the next, since this bears on the problem of mantle dynamics. That is, lateral differences in the mantle at such great depths can only be transient phenomena, which might either be the effect of dynamical processes taking place within the mantle, or could be thought of as the cause of mass transport within the mantle. Hence, the results of this study bear on mass transport in the mantle as well as on its chemical and physical state.

For the most part, however, we are concerned here with problems that are purely seismological in nature. We demonstrate that the observed travel times, phase velocities ($dt/d\Delta$), and the mean trend of the variation of amplitude with both distance and frequency can be explained in terms of physical properties of the mantle. This provides a satisfying verification of the consistency between various methods used to obtain mantle structure and resolves some of the uncertainties as to the origins of the complicated variations of amplitude of both the first and the later arriving body-wave phases.

In addition to the travel-time and amplitude data used to obtain compressional-wave velocity and Q as functions of depth, we have also applied other constraints to the inverse problem in order to reduce the number of possible solutions. In particular, we have made use of P_n and P delay data to limit our solutions. Although there is always a range of structures for any given profile that fit the data within its range of certainty, we find that the set of models implying plausible physical conditions in the mantle is quite small.

Because of the difficulties of resolution and lack of uniqueness inherent in seismic methods, we can only regard the seismic models obtained in this study to be approximations for a laterally inhomogeneous earth, to be modified in a manner consistent with additional seismic data and all other pertinent geophysical, geological, and geochemical information. In this regard *Archambeau et al.* [1968] have discussed the results of the present investigation in the context of a broader integrated geophysical study. They find that the four mantle models obtained here are quantitatively consistent with other geophysical information (such as heat flow and gravity) pertinent to the regions studied.

We have structured our discussion so that methods and procedures are separated from results as much as possible. In the following section we discuss the mantle provinces studied and the problems of distinguishing separate regions. Next we describe our procedures for analysis and inversion. These latter comments are meant to be indicative of the systematic approach to travel-time analysis used. This section can be omitted without loss of continuity by the reader interested only in the results of this study. The next four sections present the data and their interpretation in terms of mantle velocity structure for the four profiles studied. A separate section is devoted to determination of the variation of Q with depth using the frequency dependence of the observed amplitudes. The final section is a summary of results and a discussion of some of their implications. Some comparisons with the data and results of studies similar to this one are included.

Mantle Provinces

The approach we adopt is basically a straightforward iterative process of fitting theoretical travel times and amplitudes of compressional phases to the observed data. We have used compressional phases from the Shoal and Bilby nuclear explosions in Nevada and from the Fallon earthquake, which occurred at the Shoal site, to determine compressional velocity as a

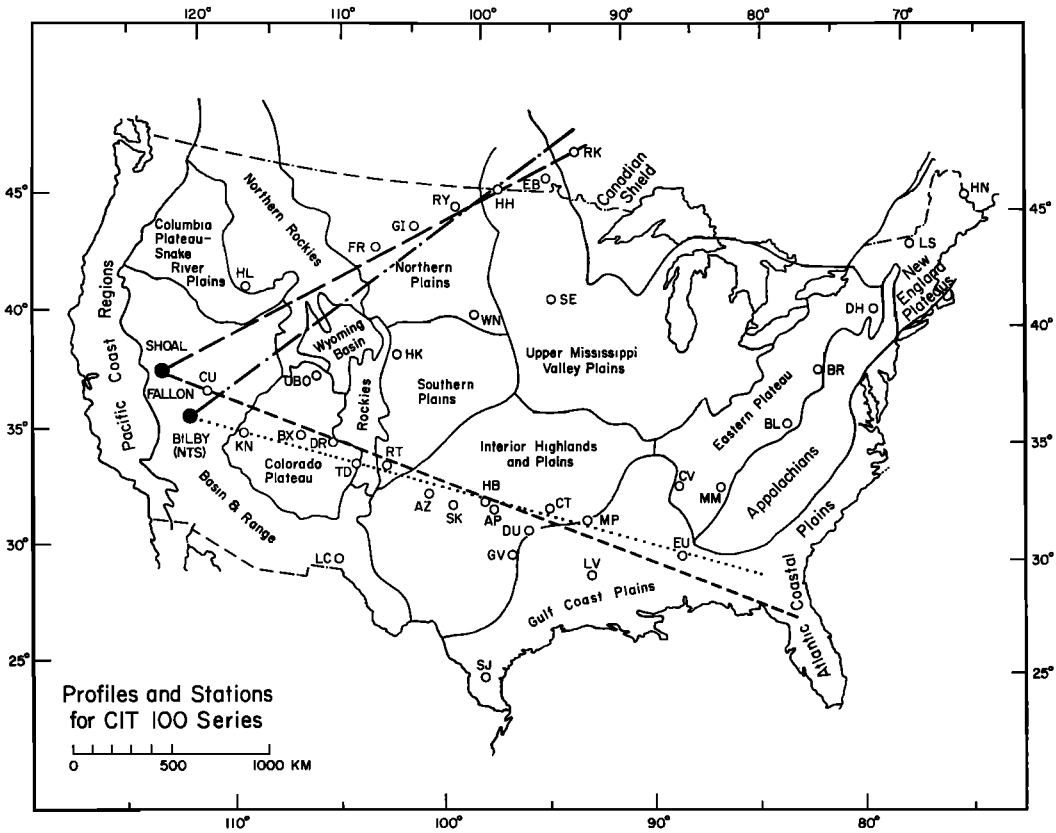

Fig. 1. Distribution of seismic stations and sources with respect to physiographic provinces of the continental United States. The lines indicate the regions sampled by the four groups of stations used, which we designate as the Shoal-Fallon NE profile (long dash), Shoal-Fallon SE profile (short dash), Bilby NE profile (dash-dot), and Bilby SE profile (dots).

function of depth along several profiles that cross distinct geological provinces. The locations of these profiles relative to physiographic provinces within the continent are shown in Figure 1.

We have interpreted the data on each profile independently in an effort to resolve the mantle structure appropriate to particular mantle provinces. We assume as a first approximation that these mantle provinces are in spatial correspondence with the surficial physiographic provinces. Although such correspondence is not known a priori, of course, it is reasonable to assume that variations in the physiographic and crustal properties are manifestations of variations in upper mantle properties. There is, in fact, considerable evidence that suggests that this is the case, as has been pointed out by numerous authors [e.g., *Hales et al.*, 1968]. A summary of the P_n velocities in the major tectonic provinces of the continent, shown in Figure 2, illustrates the correspondence between patterns of compressional-wave velocity at the top of the mantle and the boundaries of the provinces in Figure 1. The anomalously low P_n velocities shown are quite closely confined to the Basin and Range province, and, judging from the lateral gradients implied by the P_n velocity contours, the transitions in mantle properties at the boundaries of the Basin and Range province should be about as sharp as are the transitions in physiography and crustal properties (if the P_n velocity is assumed to be indicative of the upper mantle structure as a whole). The Rocky Mountain region is marked by intermediate P_n velocities of about 8.0 km/

sec, and the plains and shield both have high-velocity lids on the mantle with velocities from 8.1 to 8.2 km/sec.

In general, the boundaries of all the provinces seem quite well defined by rather rapid changes in P_n velocity. It is reasonable to suppose that this behavior is indicative of rapid changes in the whole upper mantle at such boundaries. The plains and shield appear to be one single mantle province, however, since there is a rather small variation of properties at the border between them [*Lewis and Meyer*, 1968]. The *P*-wave travel-time anomalies also show this effect. Figure 3 shows the compressional-wave delays relative to standard travel times, as determined by *Cleary and Hales* [1966], contoured on an 0.2-second interval to bring out spatial relationships. The patterns and anomalies correlate with the provinces roughly to the same degree as the P_n velocities. Correlation with structural features of smaller dimensions, such as the Sierra Nevada Mountains, is also evident, and, clearly, variations in the crust as well as the mantle affect the delays. With the exception of mountain ranges, corrections for crustal properties do not greatly change the picture. Thus, when the crust is 'stripped off,' the mountain regions appear to have early arrivals relative to neighboring regions, which implies high average velocities for the upper mantle; the Basin and Range would have an even slower upper mantle, and the Shield and Plains would still be very fast. Consequently, we see a strong correlation between P_n velocities, *P* delays in the mantle, and the physiographic and geologic provinces.

We therefore can reasonably conclude that the data from each profile are the result of sampling rather distinct mantle provinces. If the upper part of the mantle is most variable between the provinces, i.e., if there are rapid transitions at the boundaries, then we should

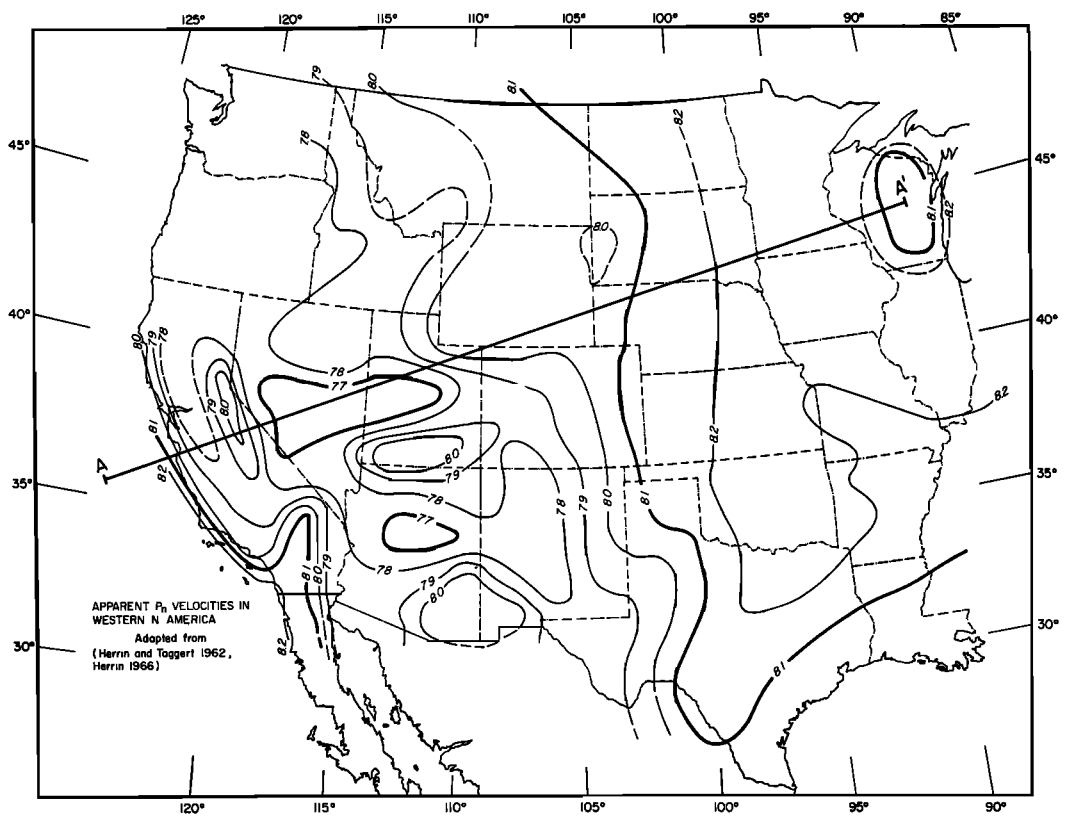

Fig. 2. P_n velocity contours for the western and central United States, from *Herrin and Taggart* [1962], with minor modifications and updating.

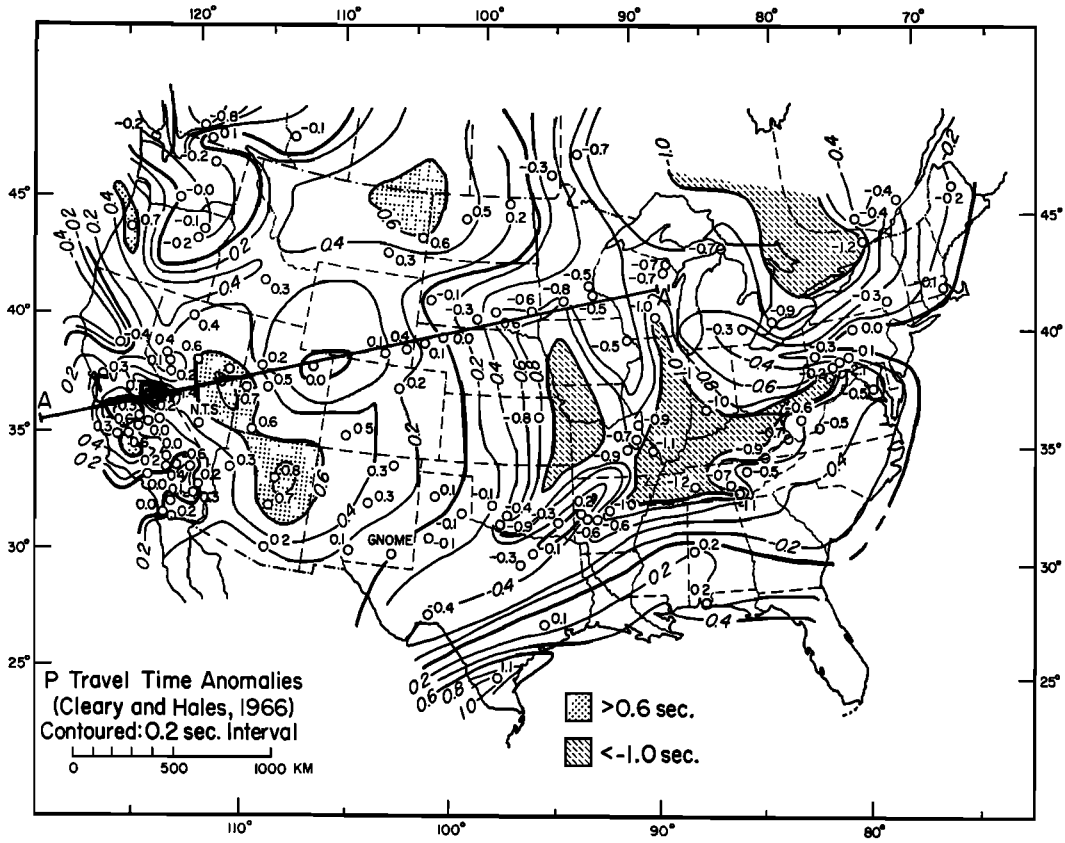

Fig. 3. Relative travel-time anomalies for compressional waves contoured on a 0.2-second interval to bring out spatial relationships, data from Cleary and Hales without modification. The data reflect both crust and mantle differences in velocity structure.

see continuous travel-time curves with rather sharp breaks as we proceed to greater distances along a given profile, the breaks being due to sampling different structures. These rapid transitions in the travel-time curves would reflect the fairly sharp boundaries of the mantle provinces and the fact that both the travel times and the amplitudes are most affected by the structure in the region at and near the bottom depth (turning point) of the ray path. As a rule of thumb, therefore, we can say that the structure sampled by a given ray is predominantly that between the source and half the distance to the point of observation, since in our particular study the more distant half of the ray path is a shield-type structure in each case. The midpoint distance corresponds roughly to the point on the surface below which the ray bottoms. A more precise description of the regions sampled will evolve in the course of the analysis of the separate profiles. In any case we expect the profile southeast from the Shoal-Fallon source to provide a good sampling of the Basin and Range upper mantle, the profile southeast from Bilby a sampling of the Colorado plateau and Rocky Mountains, and the Shoal-Fallon and Bilby profiles to the northeast a sampling of the Snake River plains–northern Rocky Mountains and the eastern Basin and Range–northern Rocky Mountains provinces, respectively. For all the profiles we expect to see changes in the travel-time curves (time delays or advances) for distances beyond about 2000 km from the source, corresponding to the sampling of a substantially different mantle province at greater distances.

In view of the limited distance range of our stations and the probable transitions in mantle

structure along the individual profiles, we can only hope to observe lateral variations in mantle structure above depths from 300 to 400 km at best. At greater depths we are sampling essentially the same province on all profiles and any differences in deep structure obtained would be due to the differences between the mantle near the source and the receiver regions.

Methods of Analysis and Inversion

The velocity structure for each profile is determined by iterative procedures applied successively to the travel-time ($T - \Delta$) data and the spectral amplitudes of the first and later arrival compressional phases. Our procedure is to adopt a starting model incorporating both elastic and anelastic parameters (v_p and Q_p as functions of depth) and to fit the travel-time data as a first step. In this process the amplitude data are initially used in a qualitative way to help fix the positions of cusps in the multi-branched travel-time curves as well as the crossover points for the different first-arrival branches. Figure 4 illustrates this stage in our iterative procedures. We also constrain our models to give a P_n velocity that is compatible with the appropriate P_n velocities obtained from Figure 2, and the mantle P delays implied by the observations of Cleary and Hales, shown in Figure 3. We have found that our P_n velocity observations are quite consistent with the P_n velocities in Figure 2, and computed delays from mantle models fitting our data easily fall in the range implied by the P delays in Figure 3. In other words, we have no difficulty satisfying these constraints with models generated from our data.

After obtaining a good fit to the travel-time data, we adjust the fine-scale features of the model, in particular the velocity gradients and the Q variation with depth, to fit the details of the amplitude observations. This final stage of

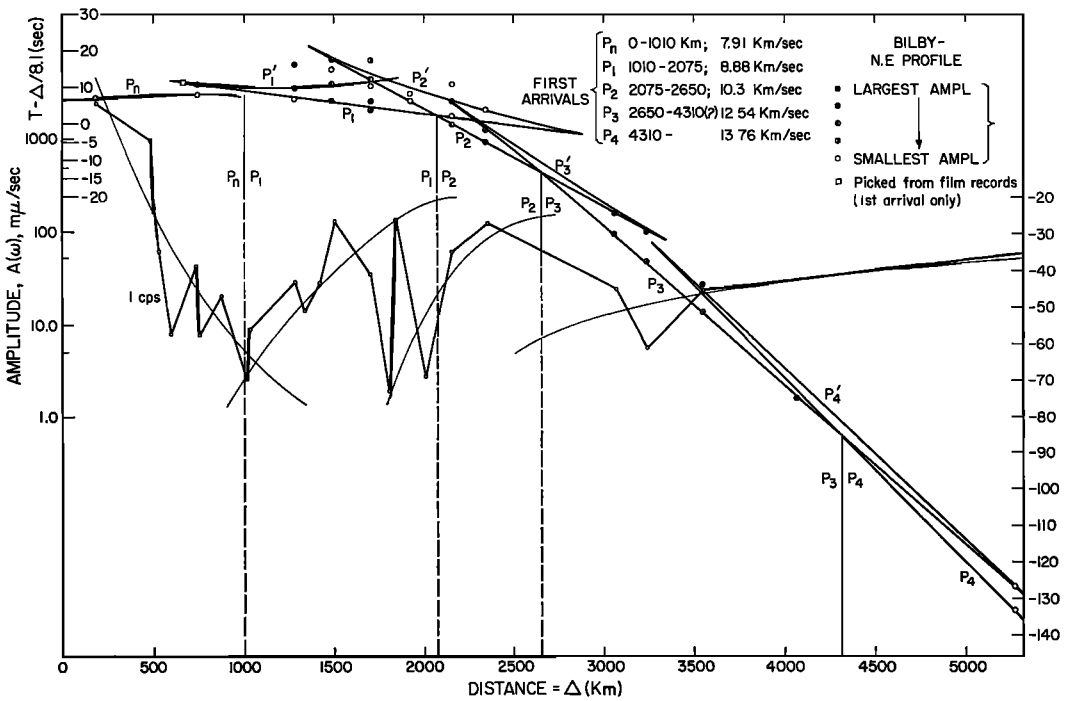

Fig. 4. Travel times for all phases and amplitudes of first arrivals (at 1 cps) as a function of distance. This is an example of the method used to select a starting model. The positions of first arrival branch intersections are determined from discontinuities or rapid variations in both the amplitude and the slope of the travel time which are well correlated with later arrivals. Inferred variations in amplitude with distance are indicated by smooth light lines. The phase symbols indicated (P_n, P_1, P_1', etc.) are used to label the distinct branches of the travel-time curve. The corresponding regions of bottom depths are shown in Figure 34.

iterations results in only second-order changes in the model. This approach is made possible only through use of a high-speed computer, which allows both trial and error and systematic iteration techniques to be employed.

A systematic procedure for inversion of travel-time and amplitude data for any collection of body-wave phases is described in Appendix 1. This constitutes the logical basis for our iterative procedures. We make use of the fact that small changes,

$$\delta\alpha_k \ (k = 1, 2, \cdots, N),$$

in the set of parameters describing the velocity variation with depth are related to the time residuals δT_Δ, defined as the difference between observed and computed travel time at a distance Δ, by [*Archambeau and Flinn*, 1966]

$$\delta T_\Delta = \sum_{k=1} \left(\frac{\partial T}{\partial \alpha_k}\right)_\Delta \delta\alpha_k \qquad (1)$$

The 'partial derivatives' of travel time with respect to the velocity parameters at fixed distance Δ are given by

$$\left(\frac{\partial T}{\partial \alpha_k}\right)_\Delta = -2 \int_{r_p}^{R} \frac{1}{v} \left(\frac{\partial v}{\partial \alpha_k}\right) \left[\frac{r^2}{v^2} - p^2\right]^{-1/2} \frac{r\, dr}{v^2} \qquad (2)$$

an integral that is easily computed numerically. The set of parameters α_k might be, for example, the expansion coefficients of the velocity in a series of suitable functions of radius. Possible representations of the velocity in analytic form are given by *Archambeau and Flinn* [1966], *Julian and Anderson* [1968], and in Appendix 1 of this paper. These relations have recently been used by *Hales et al.* [1968] to estimate the effects of structural variations on P delays.

All the quantities appearing in (2) are appropriate to the unperturbed theoretical model, r_p being the bottom depth of the ray, p the ray parameter, and R the radius of the earth. The integral is expressed for a surface source, but its form does not change for a source at arbitrary depth.

Similarly, we have for the amplitude residuals δA_P for a particular branch (say the Pth) of the travel-time curve

$$\frac{\delta A_P}{A_p} = \sum_{k=1}^{N} \left(\frac{\partial \log A_P}{\partial \alpha_k}\right) \delta\alpha_k \qquad (3)$$

where

$$\frac{\partial \log A_P}{\partial \alpha_k} = \frac{1}{2} \frac{d^2}{d\Delta^2} \left(\frac{\partial T}{\partial \alpha_k}\right)_\Delta \Big/ \frac{d^2 T}{d\Delta^2} \qquad (4)$$

Perhaps the major problem in the present analysis is that of isolating and identifying the seismic phases. This procedure can be elevated above the level of a subjective art through the use of digital filtering methods, of which the more useful are (unfortunately) nonlinear. In spite of the drawbacks of nonlinear filters, one of the more successful of this class is the polarization filter [*Archambeau et al.*, 1965, 1966]. Such filters pass vector wave forms having a given polarization and angle of emergence and attenuate wave forms corresponding to all other polarizations and emergence angles. We have used this type of filter to determine the arrival times of the later phases and their time durations, the time duration being required in the computation of amplitude spectra (because of the nonlinear response of these filters we cannot compute the amplitude spectra from the filtered record). Examples of the use of these filters have been given by *Archambeau et al.* [1966] and by *Lewis and Meyer* [1968] in studies similar to the present work. Details of the design of these filters can be found in these references. To some extent the uncertainties associated with phase identification can be reduced by the use of such methods alone; whereas the shear-wave and surface-wave energy generated near the receiver can be severely attenuated (so that only compressional waves in a narrow range of emergence angles are passed by the filter), we must still distinguish between later phases that are the result of multiple reflections in the crust at the source and receiver and later arrivals that are due to multiple paths in the mantle.

Since we have reasonably good knowledge of the crustal structure at the Shoal and Bilby explosion sites, it is possible to compute the theoretical times for the multiple reflections at the source and to eliminate them from further consideration. Figure 5 illustrates how this was done for the explosive source seismograms. For these sources the radiation pattern for P waves is nearly independent of emergence angle, and so a theoretical source function modified by the crustal transfer function, which includes reflections at discontinuities, was used to corre-

late both wave form and arrival times with multiple crustal reflections in the original and filtered records. In Figure 5 the phases on the records that match in wave form and arrival time with various crustal reflections at the source are indicated by the darkened areas in the upper group of three traces. If the synthetic seismogram is shifted to the time of arrival of other interfering body wave trains, such as *PP*, *PPP*, or *PcP*, then additional multiples can be identified. This is illustrated in the second group of three traces in Figure 5. Thus the reverberations due to layering at the source can be largely eliminated. Nearly all the remaining arrivals should be due to true multiple branches of the *P* travel-time curve or else to reverberations at the station.

Since the crustal layering at the individual stations is highly variable and in most cases poorly known, we have not attempted to eliminate these crustal reverberations directly. Instead, all the arrival times of phases not identified as *PP* and *PPP* are plotted for all the stations, and it is then possible to eliminate most of the station reverberation effects, since the crustal reverberations have a pattern in the time-distance plane different from phases associated with multiple branches, and, more important, they have markedly different amplitude characteristics. For example, referring to Figure 4, we conclude that the arrivals following P_n in the range around 800 km are P_1' mantle arrivals and not P_n reverberations since they have amplitudes that are more than ten times the P_n amplitudes, and also because they are correlated with other large-amplitude phases at greater distances.

Near caustics it appears that compressional-wave energy is spread out in a long, rather complicated oscillatory wave train, which, because of the interference effects, comes out of the polarization filter used in the form of a series of isolated pulses. At such distances we get a number of spurious arrivals following the real arrival defining the cusp, together with an estimate of the signal spectrum that is too small. This phenomenon can be recognized when all the station arrivals are plotted in the time-distance plane, since it occurs primarily near cusps and the spurious later arrivals are not well correlated with arrivals at other distances. On the other hand, the first arrival of the series does correlate with other first arrivals in a manner defining a cusp and a new first-arrival branch. Consequently, after correlating arrivals we can identify the spurious arrivals and to some extent readjust the amplitude spectrum upward. We nevertheless expect the variation of amplitude with distance for the various branches of the travel-time curve to be erratic because of these interference problems and also because of the great variability of the crustal transfer function.

The nature of the wave train near caustics is illustrated in Figure 6. The three examples show both the original times series and the polarization filter output. The first example at *HL-ID* shows P_n followed by a second phase group

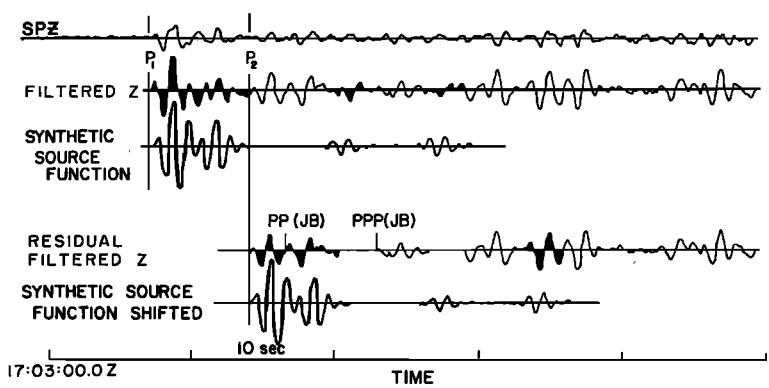

Fig. 5. Technique for identifying phases by correlation methods. In this example, both wave form and approximate arrival time are used to identify both distant reflection phases such as *PP* and *PPP* and reverberations at the source. *SPZ* denotes the original short-period vertical component of motion, and the filtering refers to polarization filtering.

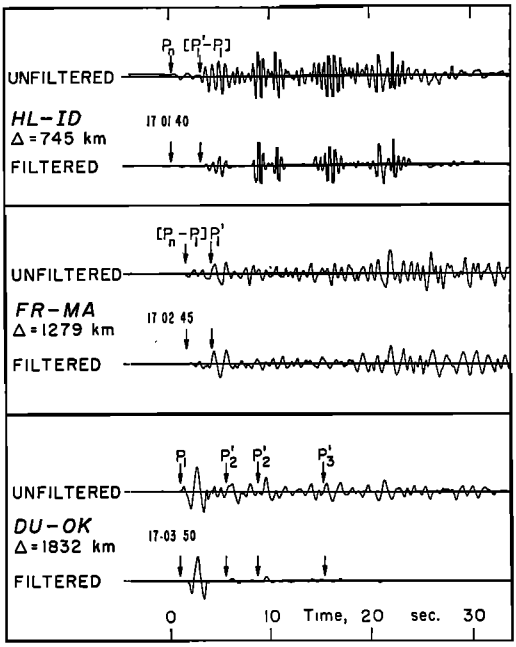

Fig. 6. Examples of the long oscillatory wave trains associated with cusps in the travel times and spurious phases remaining after filtering. The long oscillatory wave train is the P_1' phase in the first two examples.

denoted by $[P_1'\text{-}P_1]$. This bracket notation is used to indicate the possibility of two (or more) phases arriving near the time indicated. The separate phases P_1 and P_1' form a cusp in the travel-time curve at this distance and the long (20 second) oscillatory train following the onset of these phases, as previously noted, is commonly observed at caustics. This record is a typical example and shows beats in the wave train which only appear to be separate phases on both the original and the filtered records.

The second example shows a similar phenomena, but, since it is at a greater distance from the cusp formed by P_1 and P_1', the amplitude effects due to a caustic are not so pronounced. The third example at *DU-OK* shows what are probably several later phases immersed in a background of reverberations from the relatively large P_1 phase. Observations in this distance range are typically difficult to interpret since there are numerous phases all tending to have small amplitudes, the later ones being obscured by the earlier arrivals.

The theoretical amplitudes computed in this study are based on simple ray theory, i.e. geometrical spreading of energy. Naturally, these estimates will be in error for some phases, particularly near caustics. Also, we will not be able to estimate the total frequency dependence for propagational effects even if we account for nonelastic absorption. Nevertheless, ray theory provides a reasonably good estimate of amplitude, except near caustics, and, since we are considering amplitudes only in a very narrow frequency range, the frequency dependence of the elastic wave propagation effects should be about the same for all the spectral amplitudes considered. That is, the frequency dependence associated with possible leaking elastic wave effects should be much less pronounced than the dependence due to the absorption associated with anelastic phenomenon.

Since we consider the P_n amplitudes as functions of distance in detail in this study, we need to consider carefully the applicability of ray theory to interpret these amplitudes. The analytical part of the argument can be applied to other branches of the observed travel-time curve in obvious ways.

The profiles of this study all begin in the Basin and Range province and sample the upper mantle within this province or within bordering provinces. Since the temperature gradients in these provinces must be large in both the crust and the upper mantle in view of the high heat flow, we must consider the possibility that the compressional velocity gradient is negative just below the crust-mantle boundary. In addition, the possible existence of partial melting in the upper mantle suggests large negative gradients commencing at shallow depths, perhaps within 10 km of the crust-mantle boundary. Under such circumstances we must reconsider the methods to be used to predict the amplitude dependence of the P_n arrival. We surmise that, if the velocity does decrease with depth below the Mohorovicic discontinuity, then the amplitude of a critically refracted wave (head wave) will fall off more rapidly with distance than is predicted by the asymptotic head wave theory applied to a simple layered half-space (for the asymptotic theory, see *Berry and West* [1966]). In particular, the wave will continuously lose energy into the lower medium as it propagates along the boundary. This results in a frequency-dependent

attenuation with distance, with the longer-period waves decreasing more rapidly with distance than the shorter-period waves. Thus the asymptotic head wave theory for constant-velocity layers is not strictly appropriate, although a formal extension to continuous velocity variations with negative gradients is not difficult so long as the gradients are small.

On the other hand, if we consider an asymptotic wave theory leading to the classical ray theory of geometrical optics [e.g., *Karal and Keller*, 1959], we see that, if the medium is characterized by a continuous velocity variation with depth, the asymptotic theory gives a good estimate of amplitude for all types of waves under the condition that the series solution

$$\mathbf{u}(\mathbf{r}, \omega) = \sum_{n=0} (i\omega)^{-n} A_n(\mathbf{r}) \exp \{i\omega[S(\mathbf{r}) - t]\} \tag{5}$$

is asymptotic. In this expression, $\mathbf{u}(\mathbf{r}, \omega)$ is the Fourier transform of the displacement vector for the equations of motion in an inhomogeneous elastic medium, the A_n are partial wave coefficients, and $S(\mathbf{r})$ is the phase integral along the path. The series is asymptotic for sufficiently high frequencies. However, the conditions that enable us to use only the first term, which is the geometric ray approximation, can be determined by estimating the ratios of successive terms in equation 5. From Karal and Keller's results it can be shown that

$$\frac{A_1}{\omega A_0} = O\left\{\frac{1}{k_p}\left[\frac{\nabla A_0}{A_0} + \frac{\nabla v_p}{v_p} + \frac{\nabla \lambda}{\lambda + 2\mu}\right]\right\} \tag{6}$$

where k_p is the wave number ω/v_p, $v_p = [(\lambda + 2\mu/\rho]^{1/2}$, and λ and μ are the isotropic elastic moduli. Since the coefficients obey recursive relations, higher-order terms obey similar order-type relations. Thus, if the wavelength is small, the series is asymptotic, and, if the gradients of wave amplitude and elastic parameters along the ray path are sufficiently small when compared with A_0, v_p, etc., then the higher-order terms are negligible. Since the A_0 term is precisely the amplitude predicted by simple ray theory, we can judge under what conditions a purely geometrical ray approximation will be good.

For the particular case in question we are concerned with the applicability of the ray theory to what can be described as a continuously refracted wave in the region of a rapid (but continuous) increase in velocity taking place over at most a few kilometers, followed by a zone of more gradual decrease in velocity with depth, corresponding to the lid and low-velocity zones of the upper mantle. The ray theory approximation will be adequate for waves propagating primarily in regions with small to moderate grad ents typical of much of the upper mantle and should give the amplitude of a high-frequency wave with an error estimated to be less than 10% at 1 Hz. Figure 7 shows the computed ray paths for a typical structure, and it can be seen that many ray paths approximate the idealized head wave refraction paths in the region just below the crust-mantle boundary. The theoretical P_n amplitudes resulting from the ray theory approximation for these and

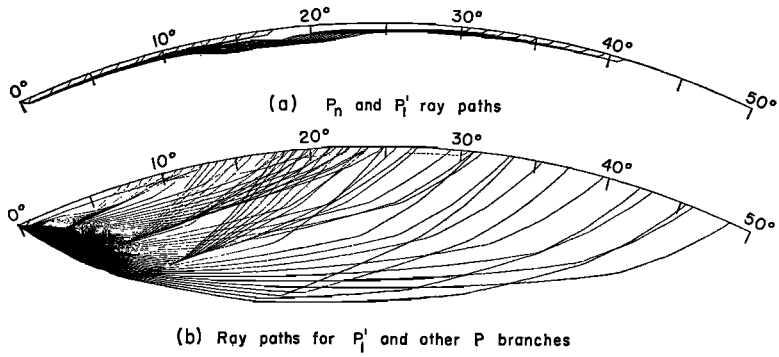

Fig. 7. Ray paths for a mantle model (CIT 109P) have a negative velocity gradient below the crust-mantle discontinuity. (*a*) The P_n branch is the first 'refraction' just below the upper boundary. The P_1' paths shown are seen to refract in the low-velocity zone and have very small amplitudes. (*b*) Ray paths for upper mantle *P*-wave phases.

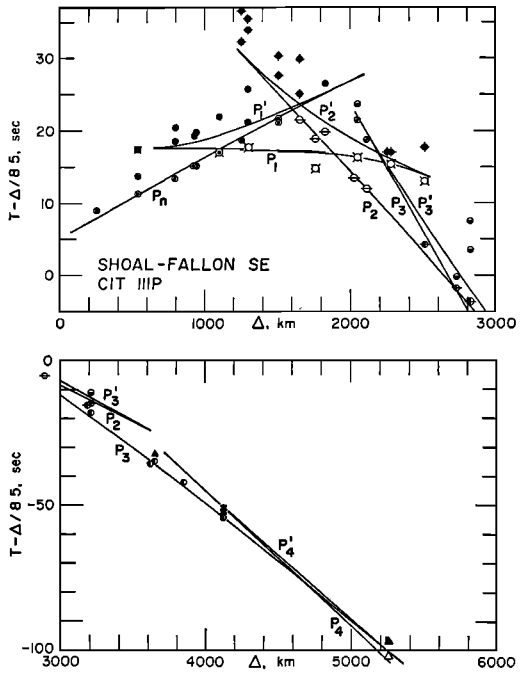

Fig. 8. Travel times versus distance for the Shoal-Fallon SE profile. The theoretical travel-time curve is generated from the model of Figure 9. Different symbols are used for observations associated with particular branches of the travel-time curve, with combined symbols where identifications are not clear.

similar ray paths fit the observed amplitude data quite well (see, for example, Figures 15, 20, and 24). Thus it appears that it is possible to obtain a satisfactory explanation of the refracted waves in this case by using only simple ray theory.

The applicability of ray theory to the prediction of amplitudes throughout the rest of the upper mantle is also governed by (6). Therefore if we apply ray theory to calculate travel times and by iterative procedures obtain a structure, we can use (6) to estimate the error we make in using the ray theory amplitudes calculated from the structure. We see, as expected, that the error is large only near caustics where ∇A_0 and the gradients of the elastic parameters are all large. Therefore in subsequent iterations of the structure to fit the amplitudes, we attempt to fit only in regions in which the approximation is quite good.

We also see that ray theory gives a valid approximation for the amplitudes, whether negative or positive gradients are involved, as long as the gradients are reasonably small, particularly in the region of the turning point for the ray. As long as equation (6) is satisfied, we can get an estimate of the refracted wave amplitude even when the gradient of the medium velocity is not small. On the other hand, the usual head wave theory for flat constant velocity layers gives much more information, essentially that information contained in several of the terms in the asymptotic series (5). However, such a theory in its present form obviously cannot be used to estimate velocity gradients without modification. It is therefore a less useful approximation than ray theory for estimating gradients of the kind likely to exist in the upper mantle.

Because we do not present all the data graphically and because we wish to make it easier for the reader to understand the numerous correlations presented here, we have tabulated all the data and pertinent information in Appendix 2, which is available on microfiche along with the entire article.[2] We have included, for all four profiles, the phase identifications (symbols and associated phase names), amplitudes at three different frequencies, and travel times with their estimated errors. In the next four sections we consider the four profiles separately.

Mantle Structure SE from Shoal-Fallon (Basin and Range)

Perhaps the most interesting region to be considered in this study is the Basin and Range province. It is a region of very high mantle heat flow [*Roy et al.*, 1968], low P_n velocity, a relatively thin 25–30 km crust, large positive mantle P- and S-wave delays [*Cleary and Hales*, 1966], and a broad negative Bouguer gravity anomaly [*Woollard*, 1966]. The region is also tectonically active, and there is evidence that the upper mantle in this region has a high electrical conductivity [*Caner et al.*, 1967]. These observations suggest high temperatures in the upper mantle with correspondingly low seismic velocities and the very strong likelihood

[2] Order from the American Geophysical Union, Suite 435, 2100 Pennsylvania Ave., N.W., Washington, D. C. 20037. Document J69-001; $1.00. Payment must accompany order.

of partial melting. We observe that the data on the profile southeast from the Shoal and Fallon sites give the best sampling of the Basin and Range province. We shall show that the best structure obtained from the data is consistent with the previous observations and their implications.

Figure 8 shows the travel-time data for this profile; at distances beyond 3000 km we have included stations not actually on the profile line. The data are denoted by special symbols according to the particular branch of the travel-times curves with which we associate each data point (Appendix 2). The travel-time curve in this figure is computed from the theoretical structure denoted by the solid line in Figure 9. This structure provides a fit to the travel times for Shoal and Fallon and to the amplitude data for Shoal, besides satisfying the independently observed P_n and P delay data. The amplitude data from the Fallon earthquake were not used since neither the spectrum nor the radiation pattern from the source itself was known, and we did not attempt to determine them in this study.

We observe that the fit to the first arrival branches of the travel-time curve is quite good, and in most cases there are second arrivals that correlate as extensions of the first arrival branches. We also note that the P_n velocity of from 7.7 to 7.8 km/sec appropriate to this region (Figure 2) is consistent with the model derived from our data. We find a mantle P delay that is also consistent with the 0.6- to 0.7-second relative delay given by Cleary and Hales (Figure 3).

The P_n branch is well observed out to 1500 km as both a first and a second arrival, and it forms a cusp with the P_1' branch. Near the left cusp of the triplication defined by P_n, P_1', and P_1, the phases defining P_1' are large, often emergent in character and rather extended in time, so that we tend to lose good definition of the first arrival time in these areas and are faced with apparent multiple arrivals due to interference effects such as were discussed in the previous section. This behavior is in general true of any of the cusps that are caustics (for example, the cusp formed by P_2 and P_2'). We have therefore adopted as best-fit models those with travel-time branches passing through the earliest of the arrivals in these regions of the time-distance plane.

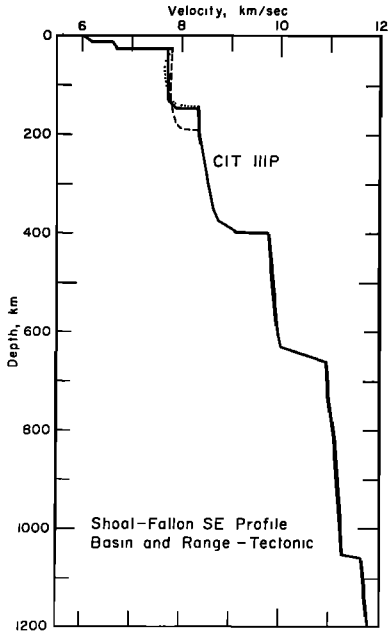

Fig. 9. Velocity structure in the Basin and Range province. Velocity-depth profiles are appropriate to the profile southeast from the Shoal and Fallon sites. The dotted curves correspond to the extreme limits of reasonable velocity variations in the upper 300 km which are consistent with the data.

We do not, therefore, regard a least-squares criterion of goodness of fit to be generally suitable to all parts of the travel-time and amplitude curves taken together; instead, we regard each branch or region of the travel-time and amplitude curves as having special characteristics that require different criteria. In particular, we use essentially a least-squares criterion for the first arrival branches and their associated amplitude curves, except in distance ranges and at stations where we expect to observe anomalous effects due to lateral changes in mantle structure or special local features in the crust at the point of observation. The early P_1 arrival near 1700 km is an example; as expected we find arrivals that are early relative to the Basin and Range travel times due to the transition to a new mantle province with higher upper mantle and crust velocities. On the other hand, the retrograde branches (denoted by primed symbols in the figures) are always fitted to the earliest arrivals appearing in the

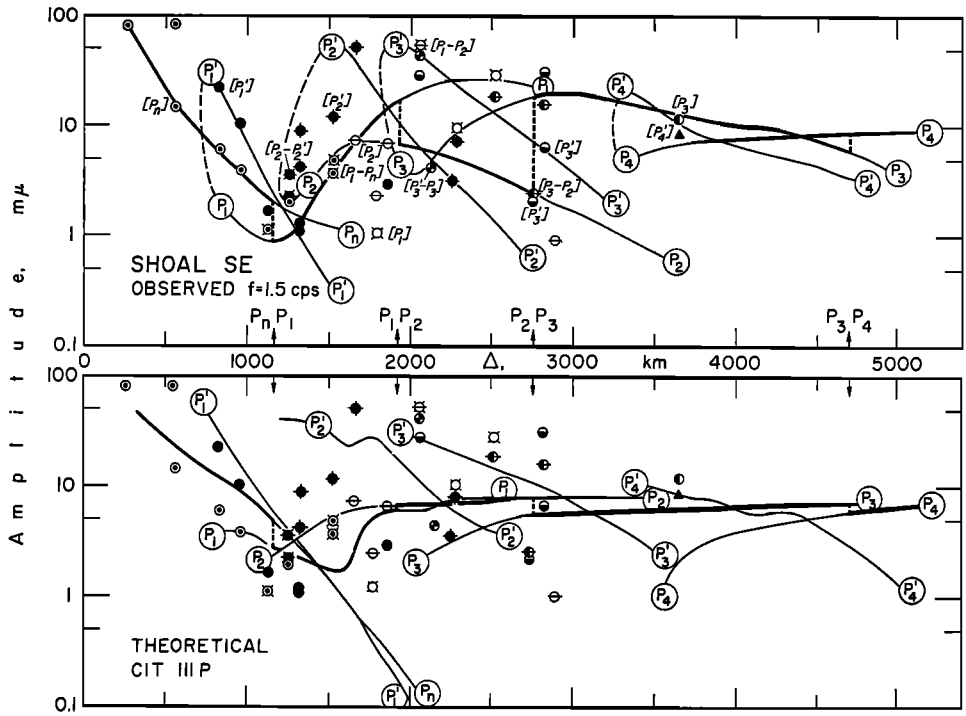

Fig. 10. Observed and theoretical variations of amplitude with distance for the Shoal-Fallon SE profile. The upper part of the figure shows the observed Shoal amplitude data and the inferred mean variation of amplitude with distance. The lower part shows the observed amplitudes and the theoretical amplitude-distance curves obtained from the structure of Figure 9 and the dissipation function of Figure 12. The heavy lines indicate the branches that are first arrivals. The symbols are the same as were used to identify the phases in the travel-time–distance plots (Appendix 2).

appropriate time-distance range, as previously noted. The tabulated error estimates (Appendix 2) reflect these characteristics of the data.

The amplitude data used most extensively are shown along with the travel-time data in Figure 10. Amplitude data have been tabulated in Appendix 2 for two other frequencies for which the estimates seem reliable. We will discuss our use of the frequency dependence of the observed amplitudes to determine absorption properties of the medium in a later section. At this stage it is important to observe that the variation of amplitude with distance for the different frequencies is very similar. Figure 11 shows the amplitude-distance data for three frequencies; we display only the first arrival amplitudes and have incorporated data from both Shoal profiles. We see that an amplitude-distance variation similar to that shown in Figure 10 holds for any of these frequencies, the only difference being in the different amplitude levels due to different source excitation and the rather subtle differences introduced by the greater absorption of energy at high frequencies. This latter effect results in the high-frequency amplitudes' falling off more rapidly with distance than the low-frequency amplitudes, giving slightly different trends to the mean variation with distance for the different frequencies.

The upper part of Figure 10 shows the observed amplitudes at 1.5 Hz. The curves shown are our inferred amplitude-distance variations along the various branches. These 'inferred' curves represent the mean observed amplitude-distance variation for each branch, and to a first approximation the amplitude data at a given frequency are seen to vary almost randomly with distance about this mean. These rapid and rather large fluctuations in amplitude

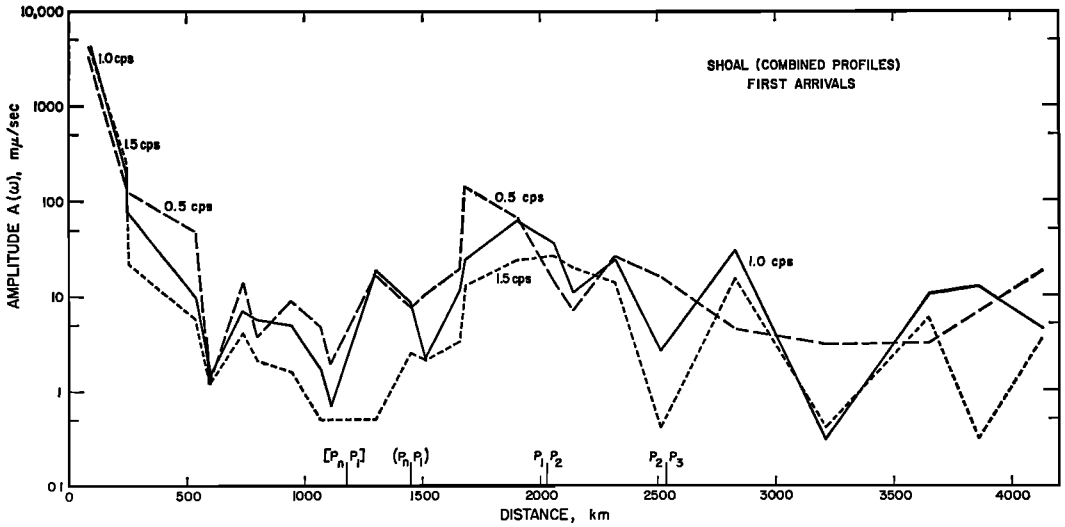

Fig. 11. Spectral amplitudes of first arrival P phases at three frequencies, as functions of distance. Each amplitude-distance curve can be considered in terms of a mean variation with distance and a superimposed fluctuation caused by variations in the crustal transfer function with distance.

are due to different crustal transfer functions for the different points of observation, as well as to interference effects from overlapping phases. The variation in the mean itself is representative of mantle properties. We therefore use this mean variation with distance as a measure of the velocity structure of the mantle.

The lower part of Figure 10 shows the theoretically predicted amplitudes on the various branches, with the observed data shown again for comparison. These theoretical amplitudes are computed from the velocity structure of Figure 9, which was also used to compute the theoretical travel times in Figure 8. For the reasons we have already discussed, no attempt was made to fit all the details of the amplitude variation. It is clear, however, that the theoretical curves have a variation with distance which is close to the observed mean curves, and the various branches have predicted amplitudes relative to each other which are in approximate correspondence to the observations. The difference between observed and predicted amplitude variations near cusps is due to the failure of ray theory in these regions. However, a higher-order asymptotic wave theory applied to the structure of Figure 9 should give an amplitude variation similar to that indicated by the observed mean curves.

Figure 12 shows the depth dependence of the anelastic dissipation parameter Q for compressional waves in the earth. This Q model,

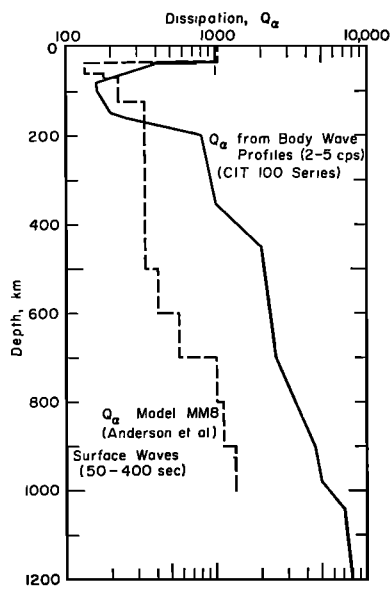

Fig. 12. Dissipation in the earth as a function of depth, inferred from body waves and surface waves. This Q variation for body waves is used throughout this study for computing the variation of amplitude with distance.

together with the velocity dependence of Figure 9, was used to fit the observed amplitude-distance data at 1.5 Hz. The Q variation inferred from long-period surface wave data by *Anderson et al.* [1965] is shown in Figure 12 for comparison. When this Q model is used to calculate the variation of amplitude with distance at the other frequencies tabulated (1.0 and 0.75 Hz), if it is assumed that Q_p is independent of frequency over this range, we obtain a fit to these data that is comparable to that obtained using the 1.5-Hz data.

In view of the nature of the amplitude data and the quality of the fit achieved, we must regard the velocity gradients in Figure 9 as rough estimates. Since the amplitude-distance data are extremely sensitive to the velocity gradients, however, even an approximate fit provides a structure whose gradients are indicative of those which actually exist in the mantle. Furthermore, the travel-time data alone, especially the character of multiplicities in the curve, also require the presence of large and rapid velocity variations near 150, 375, and 650 km.

The curves of Q_p versus depth in Figure 12 suggest that Q at high frequencies is greater than that at low frequencies. Any firm conclusion to this effect must, however, be tempered by the fact that the uncertainty in determining the Q variations either by surface-wave or by body-wave methods (particularly the method used here) is quite large. Specifically, the bounds on the two Q structures shown in Figure 12 overlap, and the differences indicated have a low confidence level. Nevertheless, it is clear that the possibility of such a difference is indeed suggested by the data. In a later section we take up the Q structure again, using a different approach, in part to try to determine whether such a frequency dependence really exists.

The uncertainty to be attached to the 'preferred structure' in Figure 9 is a matter of critical importance, especially with regard to the validity of some of the details of the velocity variation. The extreme variants shown in Figure 9 represent bounds on structures that are compatible with the observed travel-time and amplitude data within the uncertainties noted and with the P_n and P delay constraints. We have limited the possible variations as estimated from the uncertainties in the data to the upper 300 km. We conclude that the variations of structure in the depth range 300–900 km are largely due to averaging over lateral variations and, because of the observational uncertainties, are best judged from the differences between the four structures obtained for the four profiles. If there are real structural differences in the deep upper mantle between our profiles, we believe them to be less than the bounds set by the differences obtained in this study. These differences will be discussed in the final section.

We can infer from the data at least a suggestion that a short interval of high-velocity gradient exists near 1050 km. We cannot estimate any very precise bounds on the nature of this velocity variation, but it does appear likely that there are one or more zones of relatively rapid velocity increase in the region from 950 to 1150 km which are such that the velocities indicated at the two end points are achieved.

The variants indicated in Figure 9 are essentially modifications of the low-velocity region. We constructed these variants by displacing the discontinuities at the top and bottom of the zone in depth as much as possible, which has the effect of reducing or intensifying the low-velocity zone as much as possible. To a large extent the gradients in the upper 300 km were determined from the amplitude data. As is evident from Figure 9, the possible variations do not change the over-all character of the velocity variation with depth, but the uncertainty in the appropriate gradients is quite large. This is particularly true within the low-velocity zone itself.

To summarize, the characteristics of the velocity variation in the Basin and Range province of which we are most certain on the basis of our data are: the crustal thickness is 25–35 km; the velocity at the crust-mantle interface is 7.7–7.8 km/sec; an extensive low-velocity zone exists, beginning at or very near the base of the crust (within about 10 km) and extending to a depth of 150–175 km; and there is a negative gradient in the lid zone and a positive gradient in the low-velocity zone itself. These characteristics are compatible with partial melting in this zone, since strong gradients at the top and bottom of a low-velocity zone and a low velocity would result from liquid-solid phase changes. The remaining depth range,

which is, strictly speaking, more representative of neighboring provinces, has a positive velocity gradient, with rapidly increasing velocities in the range 350–425 km and again in the range 600–674 km. These transition zones are probably associated with 'olivine-spinel' and 'spinel-post-spinel' solid-solid phase changes [*Anderson*, 1967*b*]. The transition region in the range around 1050 km may be more complicated than the simple transition indicated, and in any case no physical explanation for its presence has yet been advanced.

Mantle Structure NE from Shoal-Fallon (Snake River Plains–Northern Rockies)

This profile samples the upper mantle in the Snake River plains and northern Rocky Mountain provinces, although the sampling is complicated by averaging over the northeastern part of the Basin and Range province. Although there are relatively few observations, the heat flow in both regions is about the same [*Roy et al.*, 1968], with the average near

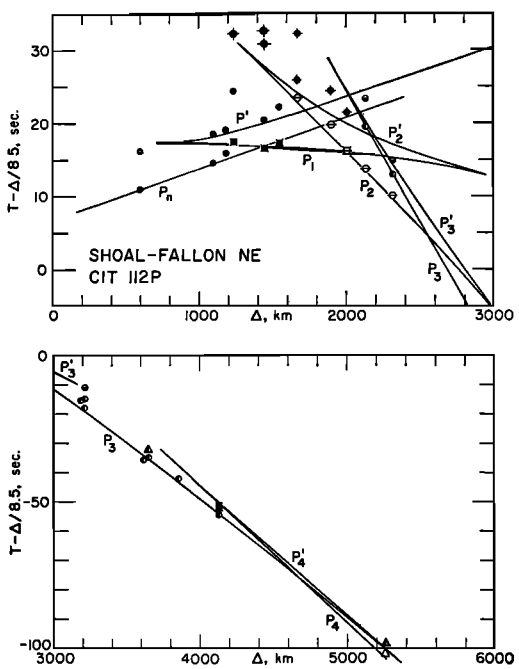

Fig. 13. Travel time versus distance for the Shoal-Fallon NE profile. The theoretical travel-time curve is generated from the velocity structure of Figure 14. Data beyond 3000 km are from both Shoal-Fallon profiles.

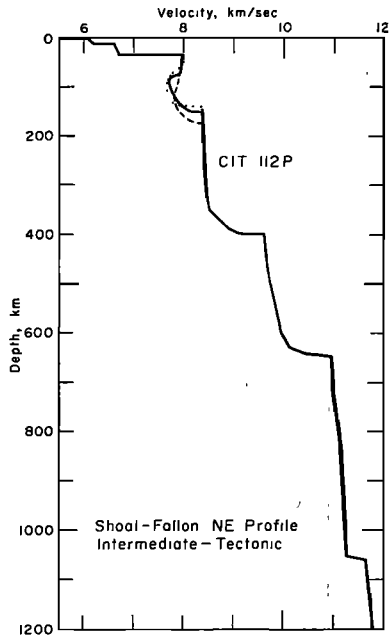

Fig. 14. Velocity structure in the Snake River plains-northern Rocky Mountain provinces, from data northeast of the Shoal and Fallon sites. The dotted curves show extreme variations of structure in the upper 300 km of the mantle.

1.5 μcal/cm^2, in contrast to the Basin and Range proper where the average heat flow is around 2.2 μcal/cm^2. The P_n velocities suggest an upper mantle 'lid' velocity of 7.9 to 8.0 km/sec, whereas the P delays show that P is only slightly late as compared with the Jeffreys-Bullen times. Relative to the Basin and Range province, P is about 0.5 second early. These observations all suggest a much less pronounced low-velocity zone in the upper mantle along this profile, although its presence cannot by any means be ruled out on the basis of these data. In the context of the over-all variation of P_n velocity, heat flow, and P delays across the near-source part of this profile, we must conclude that one or two transition zones are sampled by our data and that the resulting scatter will cause some uncertainty in the details of the velocity structure obtained.

Figure 13 shows the observed travel-time data and theoretical curves we have fitted to these data. The fit was achieved in the same way as for the previous profile, and in most respects the interpretational problems and uncertainties

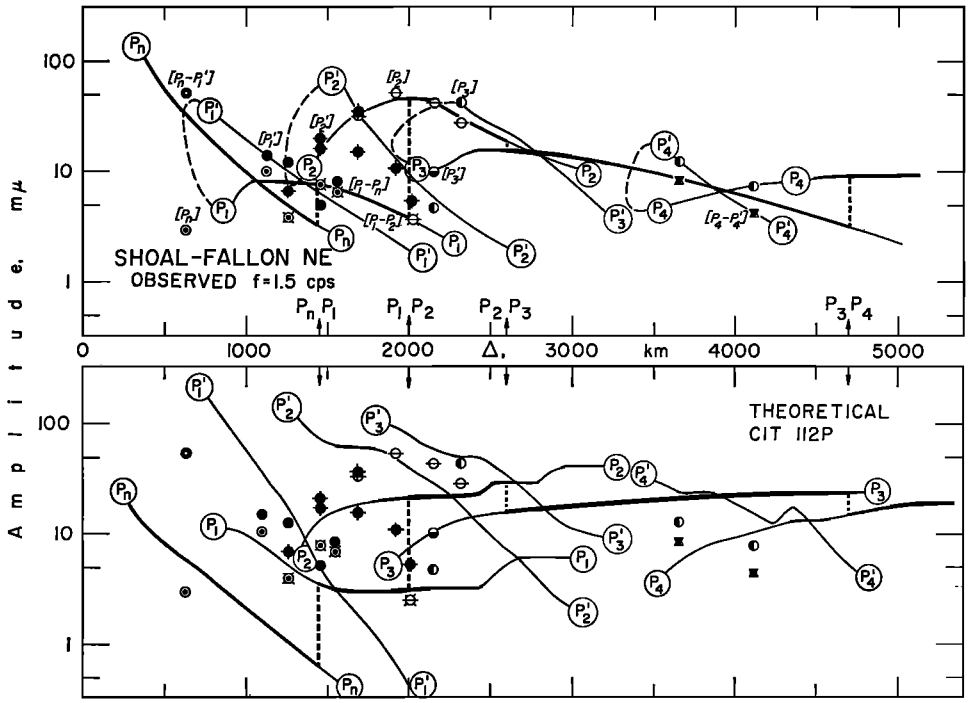

Fig. 15. Observed and theoretical variations of amplitude with distance for the Shoal-Fallon NE profile. The upper half of the figure shows the observed Shoal amplitudes and the mean variation of amplitude with distance, and the lower half shows the data and the theoretical amplitude-distance variation based on the velocity structure of Figure 14 and the Q variation for body waves of Figure 12. Heavy lines indicate first arrival branches and the heavy dotted lines connect the different branches that become first arrivals at different distances. The arrows and symbols along the distance axis show the positions of the intersections of the first arrival branches.

are the same. We note that, although the P_n data are rather sparse, they are adequate for our purposes, especially in view of the fact that the theoretical fit to these data is consistent with the P_n velocity constraint. The P_1 and P_2 branches are reasonably well defined by the data. Again the cusps formed by P_1 and P_1', P_2 and P_2' and P_3 and P_3' are caustics, and the arrivals show the same scatter in this region as the similar arrivals for the Basin and Range province. We interpret these data in the same way as we did for the previous profile.

The observed travel times and the theoretical fit for this profile are also very similar in form to that obtained for the Basin and Range profile, which reinforces our confidence in the interpretations for both profiles. It is, however, the differences between the data and the velocity structures on the two profiles that are of greater interest.

The velocity distribution obtained for this profile is shown in Figure 14, and the preferred model (which has the proper average P_n velocity and P delay) has been used for the theoretical comparison shown in Figure 13. The variant structures in Figure 14 provide an estimate of the uncertainty in this preferred structure, and on this basis the uncertainties appear to be about the same as for the Basin and Range profile. The structure obtained is most representative of the Snake River plains subprovince, but, in view of the distribution of the observations, we clearly have sampled other provinces as well. The relatively small scatter in the data implies that the other mantle provinces that may have been sampled, such as the northern part of the Basin and Range and the northern Rocky Mountains, are not much different in structure from the Snake River plains region. Of course, with more observations we might see

more scatter, but it is doubtful that such scatter would result in any major shifts in the established mean trends of the data, as would be expected to result from extreme lateral changes in the mantle.

The amplitude data for this profile are shown in Figure 15; these data were used to constrain the possible models. The rough fit to the data afforded by ray theory calculations again serves to limit the models we consider and gives an indication of the velocity gradients along this profile. The amplitude calculations were made by using the internal dissipation model of Figure 12. Since the amplitude scatter is so great, it is not possible to differentiate between different Q models for the different profiles. In what amounts to a demonstration of the ambiguity involved, we can find a whole range of Q models of the same general type as shown in Figure 12 that fit the data, but all these models have a similar depth variation and require a zone of low Q in the upper mantle.

To show the consistency between the results obtained from this profile and the previous one, we consider the spatial dependence of the amplitudes of all first arrivals at stations that recorded the Shoal event. Since this was an explosion, we expect to see a circularly symmetric radiation pattern. Figure 16 shows the result of making use of our knowledge of the distances at which various travel-time branches intersect as constraints in contouring the amplitude pattern for first arrival P waves. It should be noted that the amplitudes would hardly be contoured this way without prior knowledge of the crossover distances. Although the spatial

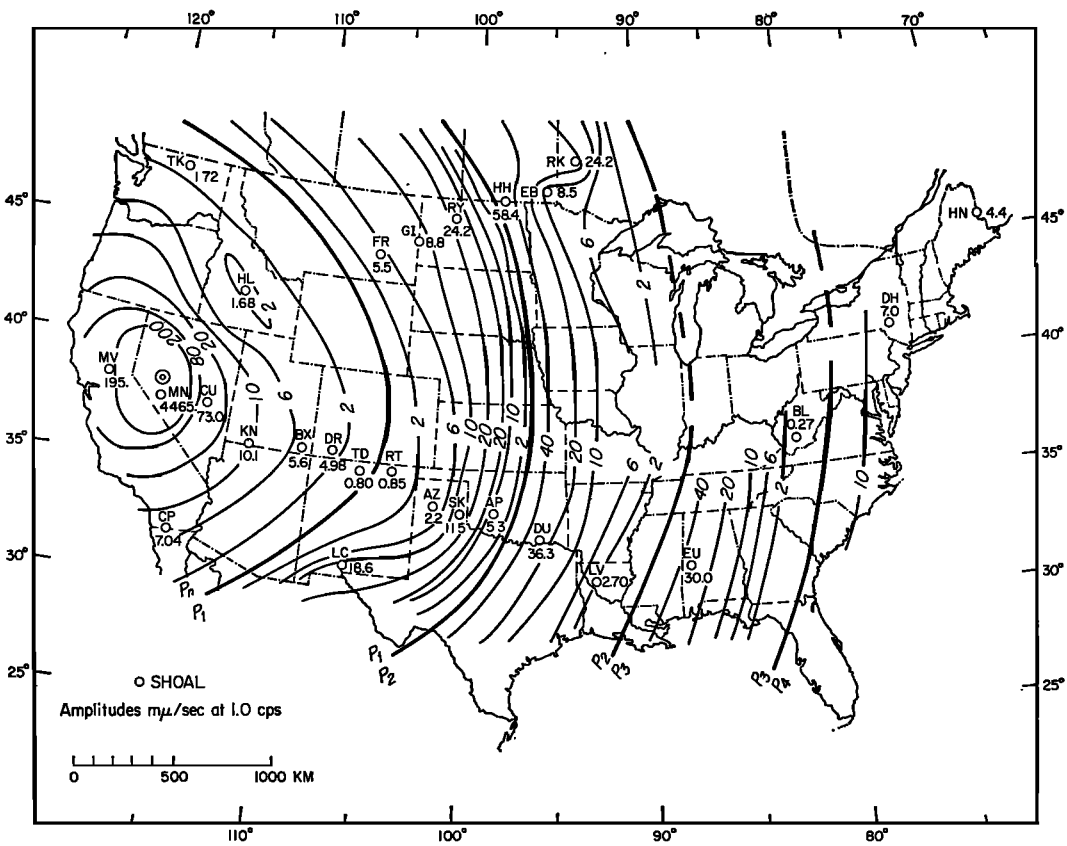

Fig. 16. Radiation pattern of the first arrival P waves from Shoal. The amplitude variation with azimuth and distance shows a strong correlation between the Shoal-Fallon profiles. The amplitudes are contoured with prior knowledge of the P-wave branch intersections (denoted by heavy lines). The circular pattern is consistent with the predicted source radiation pattern.

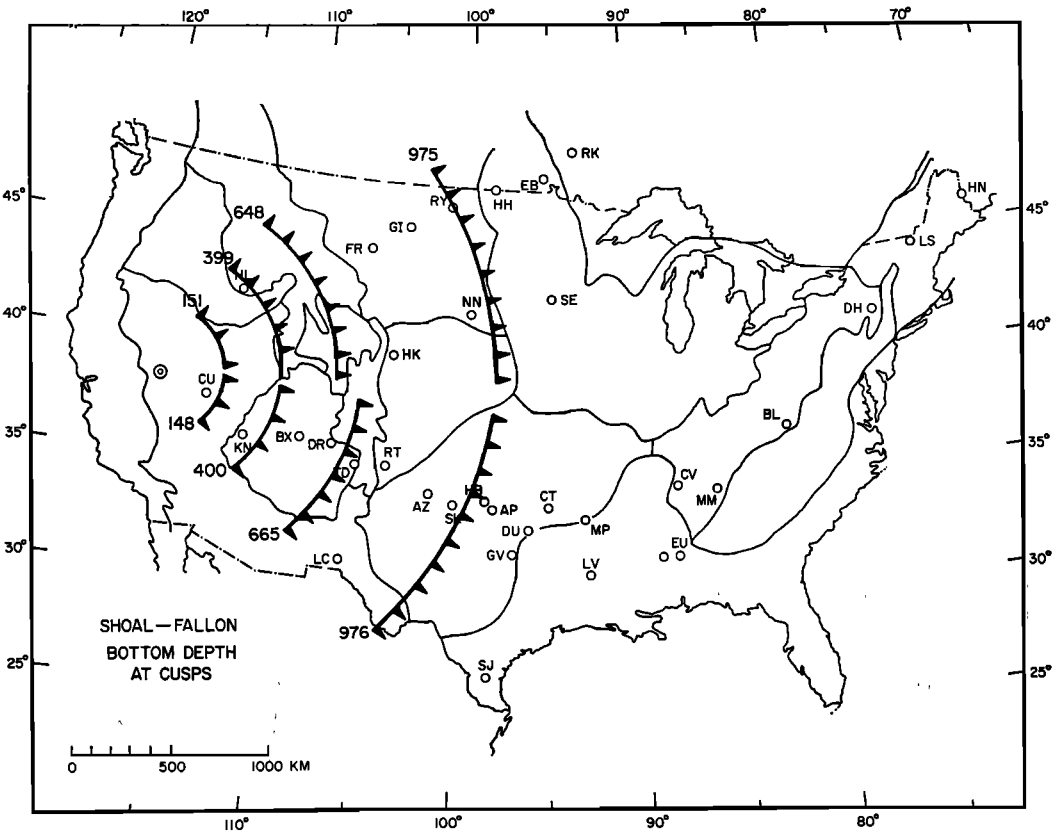

Fig. 17. Positions of ray turning points (bottom depths) at large-amplitude cusps of the travel-time curve. Depths to the turning points are indicated near the cusp lines; the hatchures indicate that arrivals on the branches forming the cusps bottom at greater distances from the source than the critical arrival at the cusp does. The depths shown are the depths to the bottoms of the low-velocity zone and the three major velocity transition zones in the mantle. The cusp line positions indicate the physiographic regions sampled by the Shoal-Fallon profiles.

correlation is quite good in detail, we cannot claim to have an overwhelming azimuth coverage, and there may be complications in the pattern not displayed by this limited amount of data. In any case we obtain the predicted result of circular symmetry, with amplitude variations along the individual branches that are predicted to first order by the mantle structures obtained. This demonstrates that the general features of the variation of amplitude with distance and azimuth can be explained in terms of properties of the upper mantle and the radiation pattern of the source. Amplitudes at other frequencies show the same general pattern, the only difference being in the over-all scaling of the amplitudes due to source excitation.

The uncertainty as to the province or provinces sampled and the extent to which we can associate our models with a particular region can now be considered in more precise terms. Figure 17 shows the positions of the computed bottom depths of the rays defining the caustics observed for both the northeast and southeast Shoal-Fallon profiles. The cusp defined by P_1-P_1', for example, depends on the velocity structure near the 150-km depth directly beneath the nearest of the indicated cusp lines. The large arrivals from this caustic are observed at about twice the 'cusp line' distance. Since the arrivals near the cusp are given considerable weight in determining the velocity structure, the nature of the low-velocity zone for the Shoal-Fallon

profile to the northeast is determined largely by the mantle near the Basin and Range–Snake River plains province boundary. On the other hand, properties of the low-velocity zone obtained from data on the Shoal-Fallon southeast profile are determined primarily by the mantle within the central part of the Basin and Range province. The P_n data along this profile sample the upper mantle 'lid' entirely independently of these cusp lines, but the first cusp line limits the geographical extent of the region sampled by the P_n wave. The other cusp lines can be interpreted in a manner similar to the first one. For all the cusps, we note that the sampling is strongly weighted by the mantle properties at distances beyond the cusp lines, since arrivals on the branches forming the cusp all bottom at depths that are either much deeper or only slightly shallower than the bottom depth of the arrival precisely at the cusp. They are therefore all strongly influenced by mantle structure near or beyond the cusp distance. We indicate this fact by hatchures turned away from the source in the figures. We conclude that the CIT 111P model is most representative of the central Basin and Range province in terms of its mantle characteristics above 300 km. Some averaging is introduced by the transition region leading to the Colorado plateau. The CIT 112P model can best be said to represent an average of the Snake River plains and northern Rocky Mountain mantles.

On comparison of the two mantle models obtained, it is clear that the major differences are in the region of the low-velocity zone. The features of the CIT 112P structure are thus essentially the same as for CIT 111P below about 200 km; above this depth, we find a termination of the low-velocity zone at about 150 km, a minimum velocity in the low-velocity zone of about 7.7 km/sec, a lid thickness of around 40 km, and an average velocity of about 7.95 km/sec. The gradient for the lid is obtained from a fit to the observed variation of P_n amplitude with distance, and the gradients in the low-velocity zone itself are obtained from combined use of the P_n and P delay constraints, the (time) position of the P_1-P_1' cusp, and the amplitude variation of P_1'. The crustal thickness is somewhat greater than that obtained for CIT 111P, which agrees with previous determinations [e.g., *Willden*, 1965] of about 35 km. The variants shown in Figure 14 provide limits on these estimates.

Mantle Structure SE from Bilby (Colorado Plateau–Rocky Mountains)

In the previous two sections we have illustrated most of the reasoning and methods used in the interpretation of our data and their inversion. The same reasoning applies to the interpretation of the data for the two Bilby profiles; therefore, we will dispense with any further discussion of these points. Since the Bilby event was larger than either the Shoal or the Fallon event, however, we find somewhat less scatter in the observed travel times and amplitude estimates, and so the amplitude data are better fitted for these profiles. The travel times also show less scatter from the theoretical fit. In general, however, the uncertainties and ambiguities are of the same general type as for the previous profiles.

The constraints imposed by the P_n, P delay, and heat flow observations in the region of the

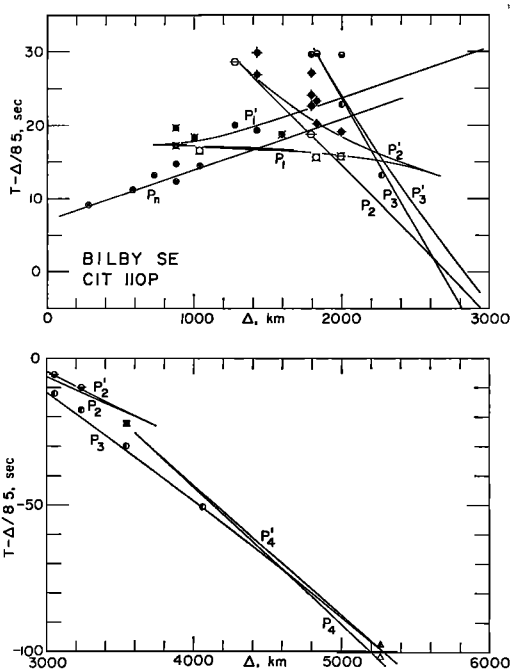

Fig. 18. Travel times versus distance for the Bilby SE profile. The theoretical travel-time curve is generated from the velocity structure of Figure 19. The data beyond 3000 km are from all the Bilby stations.

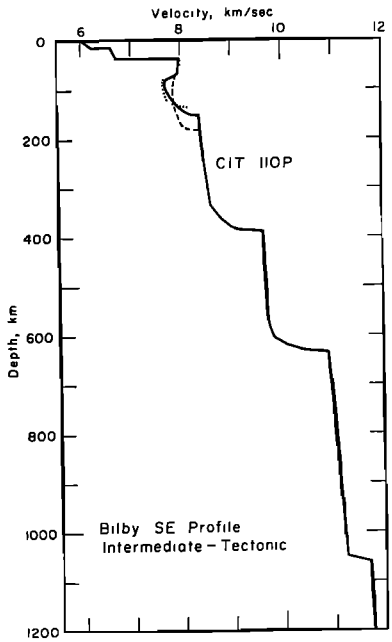

Fig. 19. Upper mantle structure in the Colorado plateau–Rocky Mountain provinces. Velocity-depth profiles are appropriate to the profile southeast from the Bilby site. Dotted curves are the extreme variations of structure for the upper 300 km which are consistent with the data. The variants are indicative of variations possible within this province.

Bilby southeast profile are: the average P_n velocity is in the range 7.9 to 8.0 km/sec, closer to 8.0; the P delay is in the range 0.5 to 0.3 second; and the heat flow is moderate, between 2.0 μcal/cm^2 in the west and 1.2 μcal/cm^2 sec in the east. In view of the previous results, these observations by themselves suggest a high-velocity mantle lid above a low-velocity zone of moderate extent, not unlike the structure obtained in the previous section. The present seismic data support this interpretation.

Figure 18 shows the travel-time data for this profile along with the theoretical fit. Again there is scatter of the data points associated with the retrograde branches, but in general we obtain a better estimate of the times for these phases than before. This results in a somewhat smaller range of models that fit the data. Figure 19 shows the preferred model and the bounds on this estimate for the upper 300 km of the mantle. We see that this model is very similar to the CIT 112P model for the Snake River plains–Rocky Mountain region.

The amplitude data, their mean trend variation, and the theoretical amplitudes calculated for the model CIT 110P are shown in Figure 20. We used the Q model of Figure 12 in the amplitude calculations. Again we must emphasize that the trend in the amplitude observations is the quantity of interest and importance here. The theoretical curves shown provide an adequate approximation to these mean amplitude relationships in view of the approximate nature of the calculations.

We should also point out that at distances where we do not observe phases at times that correspond to a given travel-time branch, we find that either the predicted amplitudes from our model structures are very small, or the predicted arrivals are close in time to later phases having large amplitudes so that they could easily be obscured by the larger arrival. On a given profile both effects occur, and not infrequently both conditions apply at once. This is particularly the case for the phases associated with the P_1 branch on all profiles.

Since we show only the variation of amplitude with distance at a frequency of 1.5 cps, it is a matter of some interest to consider the amplitude behavior at other frequencies in order to demonstrate the uniformity of the behavior of amplitude-distance observations with respect to frequency. Figure 21 shows the amplitude variation of only the first arrivals as a function of distance, for three frequencies. No attempt was made to correct for source excitation, but, if we judge from the mean amplitudes of P_n close to the source, there seems to be little dependence on frequency. However, the trends of the mean of each of the amplitude curves clearly begin to diverge in the range for which P_1 is a first arrival. This divergence is expected, since this phase propagates through the low-Q, low-velocity zone, and much of the ray path lies within this zone. As a consequence, the higher frequencies should be significantly more attenuated than the lower frequencies. This is the case of P_1 in Figure 21. For the first arrival branches at greater distances, the average Q over the propagation path will be higher than for P_1, and the differential attenuation causing divergence in the mean trends for the different frequencies should be present, but somewhat less

than observed for the P_1 branch. The observations show the expected continuation of the differential attenuation, but it is not clear that the effect is significantly less than that for P_1. Calculations using the Q model of Figure 12 and the velocity-depth model obtained yield amplitude-distance variations in substantial agreement with the observations, if it is assumed in these calculations that the Q is independent of frequency over this one-octave range of frequencies.

The structure obtained is much the same as that determined for the previous profile. The gradients in the upper 200 km were estimated in the same way as for previous profiles, primarily by using amplitudes. Again the data require that we put a negative gradient in the mantle lid region. The zones of high positive velocity gradient are located at substantially the same depths as for the previous structures. The low-velocity zone for P waves is of moderate extent. In view of the large velocity gradients, there is a strong suggestion of phase transitions at the top and bottom of the zone, the most likely possibility being the beginning and termination of a zone of partial melting. The negative velocity gradient in the lid suggests a decrease of velocity with depth due to the rapidly increasing temperature with depth in this region.

Mantle Structures NE from Bilby (Eastern Basin and Range-Northern Rockies)

The Bilby northeast profile crosses the easternmost part of the Basin and Range province, but our data are probably most greatly influenced by the upper mantle properties associated with the transition to the northern Rockies and the Rocky Mountain province it-

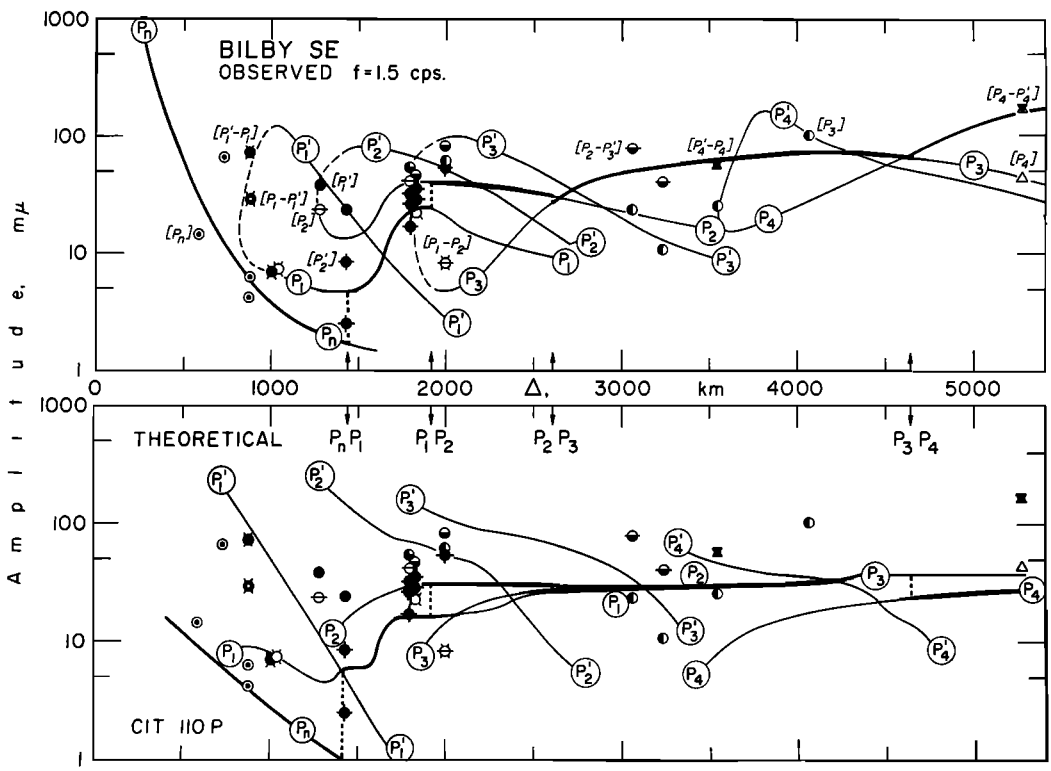

Fig. 20. Observed and theoretical variations of amplitude with distance along the profile southeast from the Bilby site. The upper half of the figure shows the observations and the inferred mean variation of amplitude that result from the deduced upper mantle structure. The lower half shows the observed data again, together with the theoretical curve computed from the velocity structure of Figure 19 and the Q structure of Figure 12.

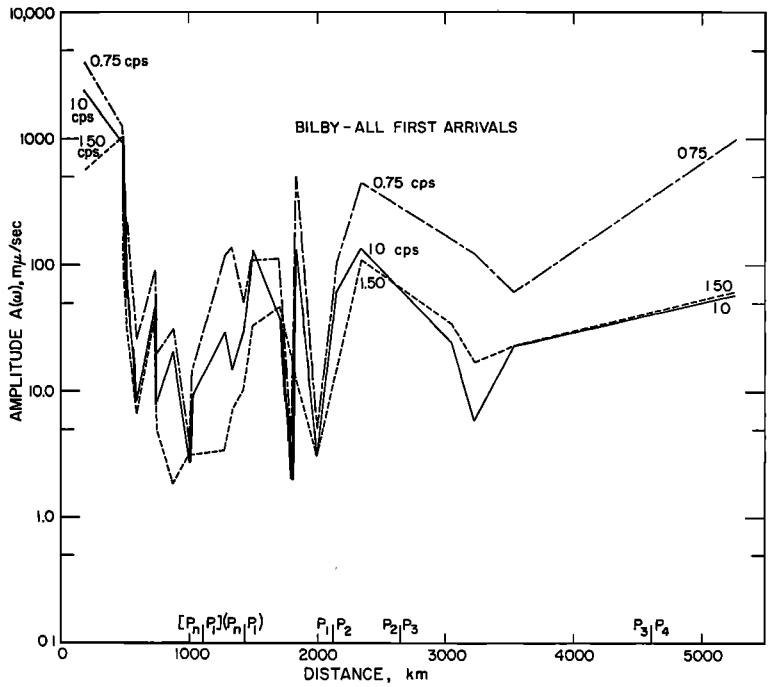

Fig. 21. Amplitudes along the first arrival branches at three frequencies, as functions of distance, for the Bilby explosion. The locations of the branch intersections are indicated on the distance axis. The differences in the trends of the different frequency curves are due to absorption, and the variation in amplitude along the individual branches is due to the variability of the crustal transfer function along the profile. The amplitude discontinuities and travel-time curves imply slightly different P_n/P_1 intersections, shown as $[P_n - P_1]$ and $(P_n - P_1)$. The discrepancy is caused by contamination of the amplitude spectrums due to interference and is typical of the interpretational uncertainties at intersections of travel-time branches.

self. The P_n velocity is therefore expected to vary with distance, but, in view of the actual distribution of stations for this profile, we should have a mean P_n velocity near 7.9 km/sec. The uncertainty in this estimate is large because of the sparseness of data in this region. This condition is indicated by the dashed P_n velocity contours in Figure 2. The heat flow and P delay data are also somewhat uncertain for this region, but they appear to show the same variability. However, as for the previous profiles, we can infer that the mean values of the P delay and heat flow are moderate, i.e., around 0.4 to 0.2 second and 1.5 μcal/cm^2 sec [*Roy et al.*, 1968]. Both imply a much less extensive low-velocity zone for P waves in this region than for the Basin and Range province proper.

The travel-time data are shown in Figure 22 along with the theoretical fit obtained from the structure CIT 109P displayed in Figure 23. We obtain a P_n velocity of 8.05 km/sec, higher than the 7.9-km/sec average for the profile, but, since most of the data defining P_n are beyond 1400 km and so in a region of higher P_n velocity than is characteristic of the Basin and Range province, we consider this higher average acceptable and so relax our constraint on the P_n velocity somewhat. The P_n arrival near 800 km is late relative to an 8.05-km/sec P_n velocity, and this could be interpreted to mean that the 7.9-km/sec velocity applies at shorter distances and that at around 800 km a transition to 8.05-km/sec velocity occurs. This would break the P_n curve into two parts, with the nearer part passing through the first two observations and the more distant part defined by the observations beyond 1200 km. We do not have enough data to conclude that such an interpretation applies; instead we must merely allow the

bulk of what data we have to fix the P_n curve. Since most of these data are at greater distances, we get a P_n velocity appropriate to the northern Rockies. Similar arguments of course can be applied to the other branches of this and the previous travel-time curves.

The amplitude information for this profile is shown in Figure 24. The mean variations in amplitude along this profile are very similar to those observed on the other profiles, and the same is true of the general features of the travel-time data. This consistency of form in the variation from one profile to the next for both the amplitude and the travel times implies that the upper mantle is similar in its essential features in all these provinces. By considering the profiles separately instead of combining all the data together, however, we can bring out systematic differences in the observations appropriate to the different regions and consequently observe the differences in the upper mantle. The significance of the fact that all the data taken together show an over-all

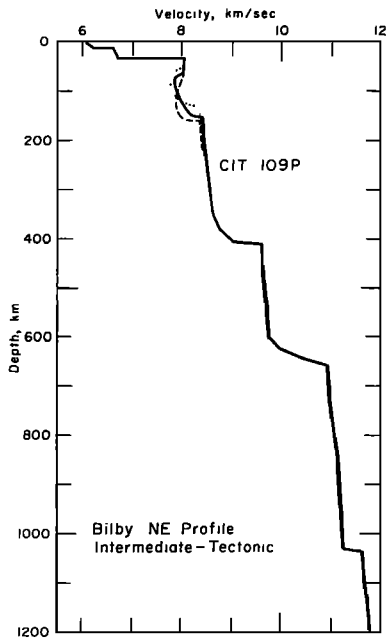

Fig. 23. Eastern Basin and Range–northern Rocky Mountain upper mantle structure. Velocity-depth profiles are appropriate to the profile northeast from the Bilby site. The dotted curves show the extremes of structural variations consistent with the data.

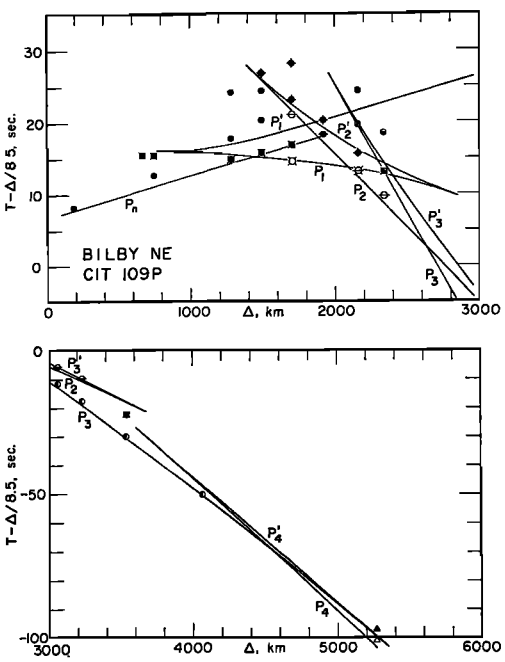

Fig. 22. Travel time versus distance from the Bilby NE profile. The theoretical travel-time curve is generated from the model of Figure 23 and the data beyond 3000 km are from both Bilby profiles.

compatibility with the structures obtained for each of the profiles is that additional observations do not change the basic features of the models obtained.

The velocity structure for this profile shows the least pronounced low-velocity zone of those obtained in this study, but in all other respects the structure is similar to the others obtained. It thus appears that the major differences in upper mantle structure from one geological region or province to the next is in the character of the low-velocity zone.

Figure 25 shows the radiation pattern of the first arrival P wave at 1.0 cps, contoured on the basis of the travel-time and amplitude interpretations of the Bilby data. Again we find a correlation between the amplitudes and the expected symmetry in the radiation patterns, as was the case for Shoal, provided that we make use of the results previously obtained as a basis for the interpretation of the spatial variation of the amplitude data. Figures 25 and 16 clearly show the strong similarities in the ampli-

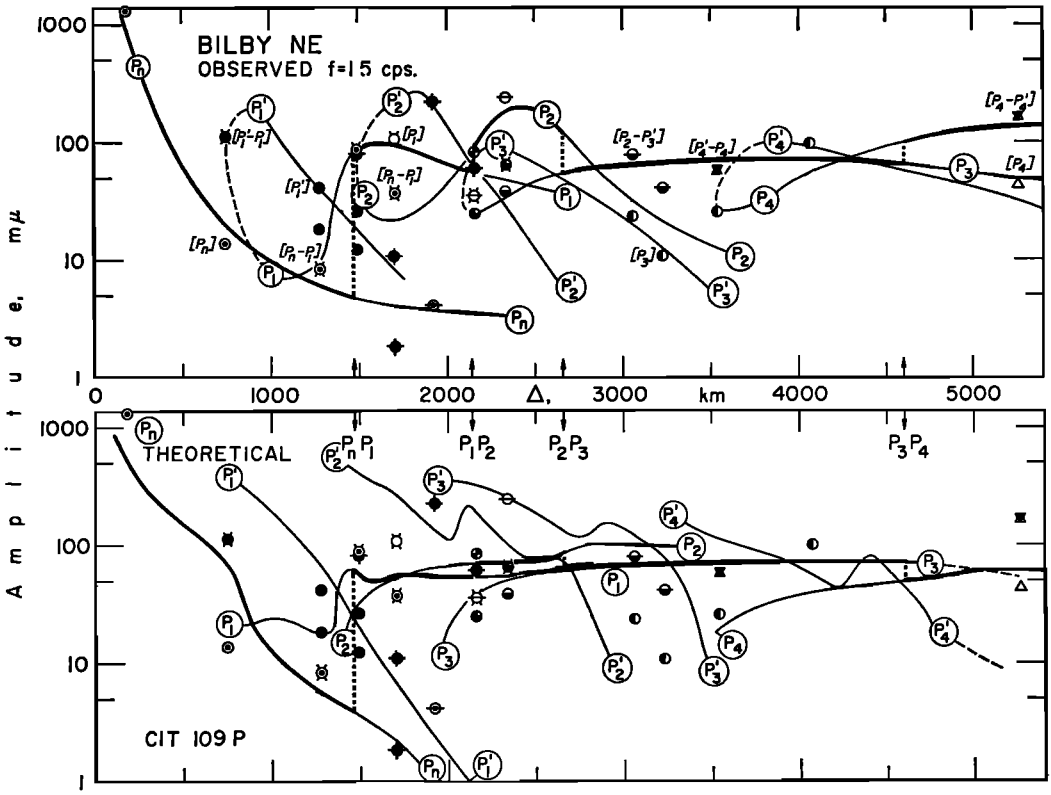

Fig. 24. Observed and theoretical variations of amplitude with distance for the Bilby NE profile. The upper part of the figure shows the observed amplitudes and their inferred mean variations with distance; the lower part, the observed data and the theoretical amplitudes calculated from the velocity structure of Figure 23 and the Q structure of Figure 12. Heavy curves indicate first arrivals.

tude variations along all the profiles studied.

Figure 26 shows the cusp lines for Bilby and the regions sampled by the Bilby profiles. We conclude that the Bilby southeast data are representative of the Colorado plateau, i.e., that CIT 110P is predominantly a plateau mantle model, whereas CIT 109P represents the northern Rockies, since the first stations recording P_n arrivals are so far from the source. As with the Shoal profiles, however, there is probably some contamination from the crust and mantle provinces on either side of these specific regions, and so the structures obtained are averages. Although we have tried to minimize the effects of lateral variations along the individual profiles themselves by taking into account the obvious transition zones and weighting the data accordingly, it is unavoidable that (as in all seismic methods) a lack of precise definition of the regions sampled will result. In comparison to other seismic methods, however, the approach used here appears to have higher resolution; in fact, only the body-wave phase velocity method appears comparable in structural resolution power.

Anelastic Properties of Crust and Lid Region of Upper Mantle

Using the travel times and amplitudes together, we have determined velocity models and a rough Q model. In the spirit of our iteration procedure, we can now use the velocity models obtained to improve on the Q model, or even in principle to obtain a Q model appropriate to each of the velocity models. The error introduced in the new Q models due to errors in the velocity models used will be of second order, and so iteration will work.

The basis of the method used to determine Q involves measuring the rates at which different frequency components fall off with distance. If we know the structure, we can calculate the amplitude decay due to propagation in an elastic medium and divide it out. The remaining amplitude decay should depend only on the absorption along the wave path. The source radiation pattern properties also affect the behavior of amplitude with distance, but for compressional phases from explosions the radiation pattern effect should be very small.

There are two major difficulties in applying what is in principle a straightforward procedure: First, we do not have a detailed knowledge of the crustal structure all along the profile, and so we cannot account for the way variations in the crustal transfer function and local scattering from inhomogeneities affect the observed amplitude-distance relations. Second, our prediction of amplitude variations due to radial and lateral velocity variations is based on asymptotic theories, which are only rough approximations, especially with respect to the frequency dependence of the amplitudes. Since we are looking for what amounts to a second-order effect, these problems limit the resolution of the method quite severely.

We use either a simple ray theory or a classical head wave theory to calculate the amplitude variations due to velocity structure and average out the crustal effects by using only the mean trend of the observed amplitude variation with distance. In addition we only attempt to obtain Q estimates from the best of the available amplitude data, in par-

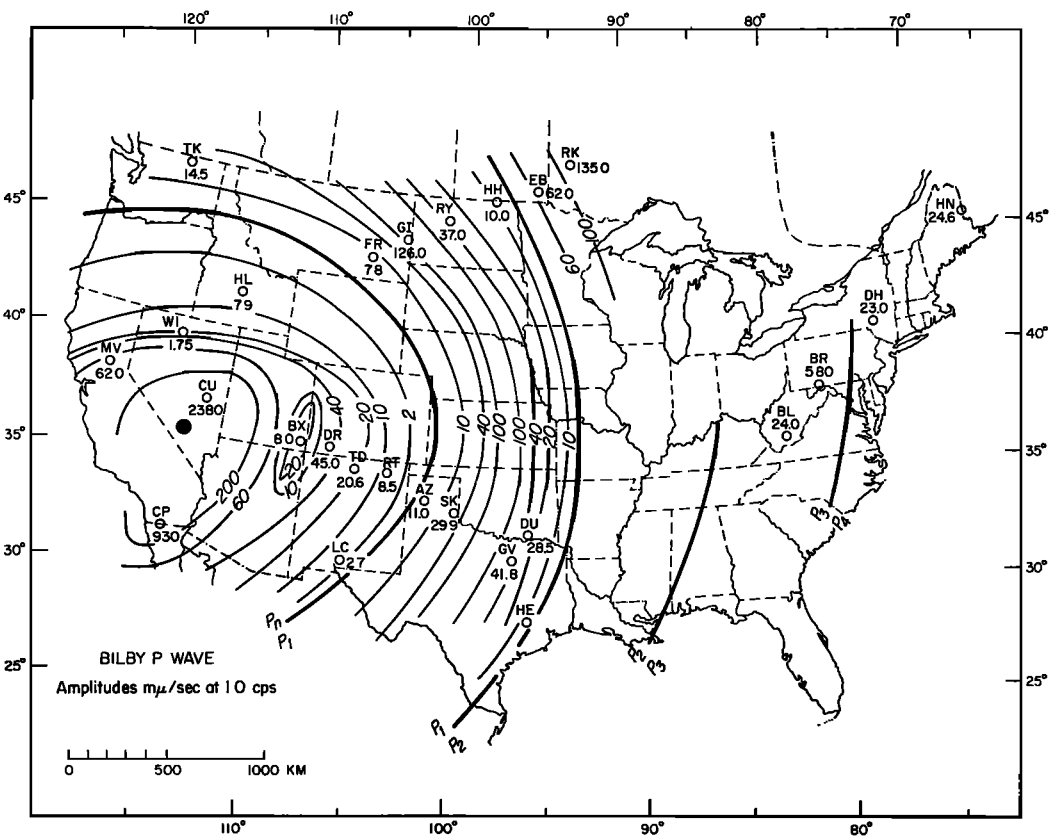

Fig. 25. Radiation pattern of the first arrival P waves from Bilby. The amplitudes are contoured on the basis of the observed P-wave branch intersections, which are indicated by heavy lines. These intersections correlate with intersections on the travel-time curves for the two Bilby profiles. The amplitude variation shows a strong correlation in distance and azimuth and is consistent with the circular pattern predicted for an explosive source.

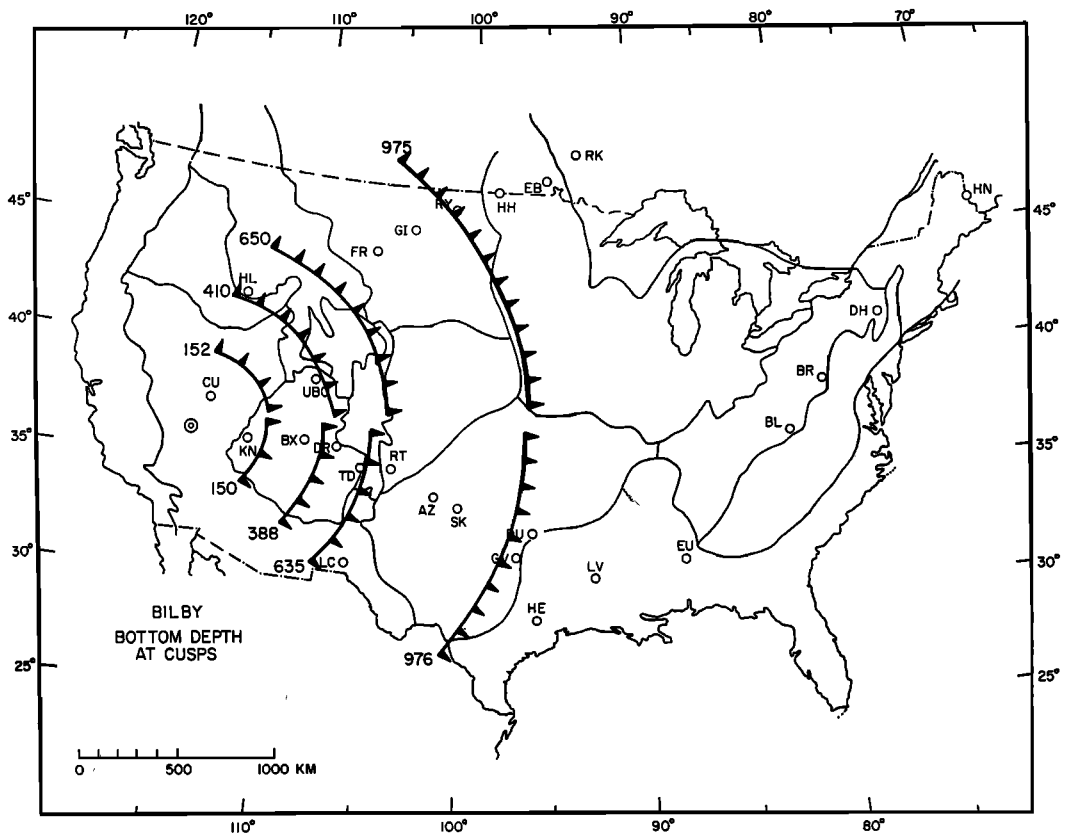

Fig. 26. Positions of ray turning points (bottom depths) at large-amplitude cusps of the travel-time curves for Bilby. Bottom depths are indicated near the cusp lines and hatchures indicate sampling at greater distances for the two branches forming the cusp. The P_n phase is controlled by the velocity structure in the mantle lid on both sides of the near-in cusp line; the other mantle phases, by structure at and beyond the appropriate cusp lines.

ticular the P_n amplitudes. Although the results must be regarded as preliminary, they nevertheless appear to imply higher intrinsic Q values at higher frequencies in the earth.

Proceeding along the lines indicated, we define an absorption parameter

$$K(\omega, \Delta) = \exp\left[-\frac{1}{2}\omega \int_{\Delta} \frac{ds}{Qv(s)}\right] \qquad (7)$$

where s denotes the path distance along a ray and $v(s)$ denotes the velocity in the medium along the ray. In addition, if we define

$S(\omega)$, spectrum of P waves from an explosive source.

$G(i, \Delta)$, geometrical spreading factor for rays with emergence or incidence angle i at distance Δ.

$A(\omega, \Delta)$, observed amplitude at distance Δ and frequency ω.

$a(\omega, \Delta)$, theoretical amplitude, assuming geometrical ray theory and attenuation.

then

$$a(\omega, \Delta) = G(i, \Delta)K(\omega, \Delta)$$

with G and K calculated from first-order velocity and Q structures.

If we consider the ratio of the observed amplitudes of a given phase at two frequencies ω_1 and ω_2 for a particular distance Δ, then we may calculate the ratios

$$R(\omega_1, \omega_2; \Delta) = A(\omega_1, \Delta)/A(\omega_2, \Delta)$$

as a function of distance from the source for a

given phase. Under the assumption that ray theory gives a valid estimate of the amplitudes over the range of Δ where we have observations, then

$$R(\omega_1, \omega_2; \Delta) = \frac{S(\omega_1)G(i, \Delta)K(\omega_1, \Delta)}{S(\omega_2)G(i, \Delta)K(\omega_2, \Delta)} \quad (8)$$

to first order. We assume that the observed amplitude spectra have been corrected for instrument response. Quite clearly the geometrical spreading factor cancels so long as this approximation is valid.

In this regard, however, we note that (8) has this form for classical head waves also. That is, the amplitude can be separated into the product of a function that depends on frequency alone and a function that depends only on distance and the critical angle. For such waves the source factor $S(\omega)$ actually would incorporate both the source spectrum and the frequency dependence of the amplitude which is due to refraction. In the following discussion we will refer to $S(\omega)$ as a source function, but it should be understood that it can be regarded in this wider sense. That (8) retains this form for simple head waves is important in this discussion, since we will apply the results to P_n. In general, the frequency and spatial dependence of the amplitudes of body phases cannot be separated from each other, and it is only when both the ray theory and the classical head wave approximations are applicable that this discussion applies.

Suppose there is available a station at an epicentral distance δ that is small in the sense that $K(\omega, \delta) \approx 1$ for all ω in the range of interest. We can in this case assume a reasonable crustal Q value (since δ is small, and only the crustal part of the path is important) and estimate the ratio $K(\omega_1, \delta)/K(\omega_2, \delta)$ with small error. In this case we can correct the observed quantity $R(\omega_1, \omega_2, \Delta)$ for attenuation and obtain

$$\frac{S(\omega_1)}{S(\omega_2)} = R(\omega_1, \omega_2; \delta) \cdot \left(\frac{K(\omega_2, \delta)}{K(\omega_1, \delta)}\right) \quad (9)$$

an estimate of the source spectral ratio, and all other separable frequency factors, which will be accurate to first order.

Therefore, we can cancel the 'source' ratio in (8) as well if we divide (8) by (9). Thus we obtain an estimate of the differential attenuation from

$$\eta(\omega_1, \omega_2; \Delta) = \frac{R(\omega_1, \omega_2, \Delta)}{R(\omega_1, \omega_2; \delta)} \cdot \frac{K(\omega_1, \delta)}{K(\omega_2, \delta)} \quad (10)$$

where the ratios of R are the observed quantities. The ratio $K(\omega_1, \delta)/K(\omega_2, \delta)$ is calculated, and for a very wide range of Q values for the crust, certainly including all reasonable values, this calculated attenuation ratio is slowly varying and very close to unity. If δ is small enough (less than 100 km), the correction is so close to unity that it may be neglected.

In any case, we have from the definition of $K(\omega, \Delta)$

$$\eta(\omega_1, \omega_2; \Delta) = \exp\left[\tfrac{1}{2}\omega_2 \int_\Delta \frac{ds}{Q_2 v(s)} - \tfrac{1}{2}\omega_1 \int_\Delta \frac{ds}{Q_1 v(s)}\right]$$

If we represent the medium by (N) layers, then

$$\frac{1}{\pi} \log \eta = \sum_{i=1}^{N} \left[\frac{f_2}{Q_i(f_2)} - \frac{f_1}{Q_i(f_1)}\right] t_i(\Delta) \quad (11)$$

where j is the layer index and $t_j(\Delta)$ is the travel time of the ray in the jth layer.

If we also assume that the intrinsic Q is independent of frequency over the range f_1 to f_2, (11) simplifies to

$$\frac{1}{\pi(f_2 - f_1)} \log \eta(f_1, f_2; \Delta) = \sum_{i=1}^{N} \frac{1}{Q_i} t_i(\Delta) \quad (12)$$

Consideration of several mechanisms of seismic-wave attenuation in the earth that appear to be possibilities at the present time [*Anderson and Archambeau*, 1964; *Jackson and Anderson*, 1970; *Gordon and Nelson*, 1966] leads us to the reasonable assumption that the variation of Q as a function of frequency is rather slow. This is even more reasonable if we consider only a narrow frequency band, so that (12) should be valid when the frequency difference $f_2 - f_1$ is not large. However, since our knowledge of the mechanism of attenuation is uncertain and only qualitative at the moment, it is not possible to determine beforehand the actual frequency range for which (12) is a good first-order approximation. We can, however, iterate toward a more precise result if we use (12) to estimate the Q in several such frequency bands, taking the Q obtained to be that representative of the mean of the frequency band. From many estimates scattered over a wide frequency range, it should then be possible to obtain at least a

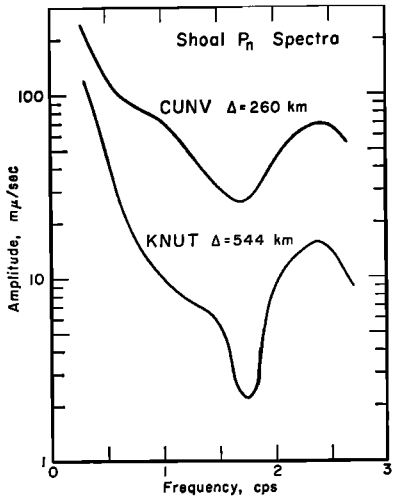

Fig. 27. Amplitude spectrums for P_n at two Shoal stations showing the regularity in the shape of the P_n spectrum as a function of distance for this phase. Station CUNV is used to normalize the more distant measurements.

preliminary estimate of the Q dependence with frequency to be used with (11) for a higher-order estimate.

The approach outlined can be applied to any of the branches of the travel time curve. As a specific example, we consider the P_n amplitudes. Figure 27 shows the amplitude spectra for P_n at two stations for Shoal. We use the nearer of these to determine the source correction along the lines previously discussed. The fact that the shape of the two spectrums shown in Figure 27 is nearly the same implies that lateral changes in the velocity structure are small in this distance range. We will therefore assume that the nearer station represents the source and the spectral ratios with respect to this station will be used to scale the amplitude ratios at more distant stations, according to equation (10).

The actual change in the spectrum with distance illustrated in Figure 27 is precisely what we expect from wave propagation in a medium of rather high Q without appreciable lateral variations and confirms our major assumptions. Thus computing the normalized spectral ratios in the manner indicated by (10), we obtain observational values of $\eta(f_1, f_2; \Delta)$ at 1.5 and 1.0 cps and at 0.75 and 1.0 cps. These values of the differential attenuation are shown in Figure 28. Using (12), we have computed several theoretical curves for various Q values for the crust and mantle lid region; these curves are also shown in Figure 28. The best fit to all the data is given by a mean crustal dissipation factor $Q_c = 1000$ and a mantle lid dissipation $Q_m = 400$. There is some suggestion of a frequency dependence, in that the data from the frequency range 0.75 to 1.0 cps can be fit equally well by the combination $Q_c = 1000$ and $Q_m = 300$, but the data are not really adequate to allow us to differentiate between the two models. In any case, we can associate esti-

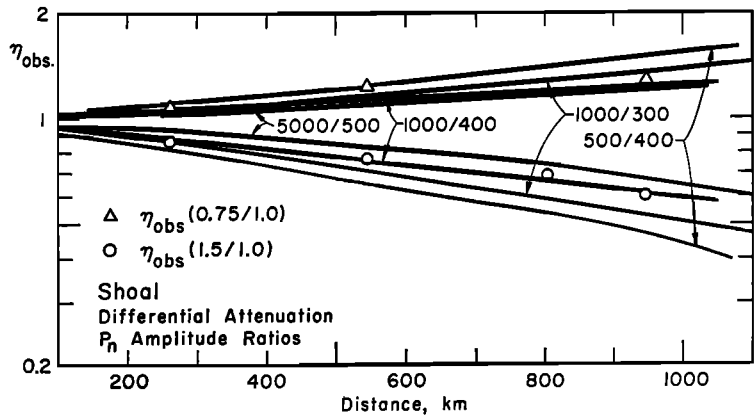

Fig. 28. Observations of the differential attenuation of P_n from the Shoal explosion in two frequency bands (0.75–1.0 cps and 1.0–1.5 cps). The theoretical curves shown are values of η computed from the different crust and mantle lid Q models; the best fit is given by $Q_c = 1000$, $Q_m = 400$. For a frequency-independent Q, both sets of data should be fitted by the same Q model.

mated Q values with the mean frequencies in our bands, so that $Q_e(1.25) \approx Q_e(0.875) \approx 1000$ and $Q_m(1.25) \approx Q_m(0.875) \approx 400$. It is significant that the data clearly require an appreciably different average crustal Q and mantle lid Q. The simplest interpretation is that the mechanisms of attenuation are thermally activated, so that Q_m represents the higher average temperatures in the lid region as compared with the average dissipation in the crust, but there are other explanations.

We can consider the amplitude data from the Bilby profiles in the same fashion. As was the case with Shoal, the amplitude radiation patterns for Bilby (Figure 25) show that the generation of P waves conformed closely to an idealized explosive source. Figure 29 shows that the shape of the spectrum as a function of distance remains basically the same over a large range of distance, indicating that there are no strong lateral changes of crustal properties. In this figure, however, we note a slight shift of the minimum in the spectrum near 1.5 cps toward a lower frequency at greater distance, the opposite of what was observed for the Shoal spectrums. A shift of minima toward higher frequencies is actually expected if the effect is due to absorption alone, so that there may be a small effect that opposes the trend introduced by normal attenuation. Presumably this effect is caused by a small difference in crustal properties. Figure 30 shows the differential attenuation data for the Bilby profiles, again with various theoretical curves for comparison. In this illustration we have chosen to display theoretical curves only with $Q_e = 500$. We could have plotted theoretical curves with $Q_e = 1000$ in Figure 30 and obtained equally good fits to the data with slightly lower values of Q_m. In particular, $Q_e = 1000$ and $Q_m = 300$ fit the Bilby data about as well as does the model $Q_e = 500$, $Q_m = 350$. This illustrates the ambiguity inherent in this particular application of the method. Of the group of models that fit the data reasonably well, however, we find that they all require a higher Q in the crust than the mantle lid. Higher Q values are also required to explain the amplitude decrements at higher frequencies. This suggests a frequency-dependent dissipation, with Q increasing with frequency. In addition, the Q models that fit the Bilby data have somewhat

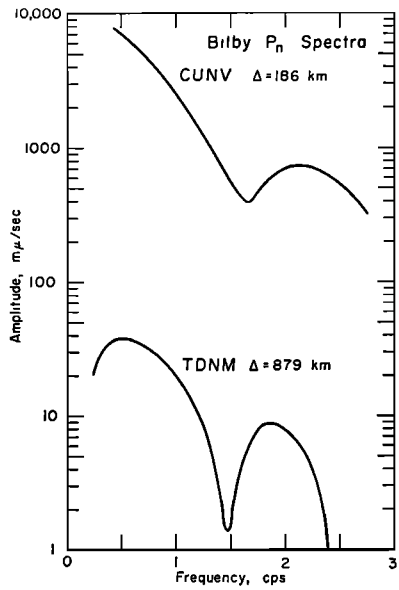

Fig. 29. Amplitude spectrums for P_n at two Bilby stations showing the regularity in the shape of the observed spectrum. The CUNV station was used to normalize the observations at greater distances.

lower values of Q in both the crust and the mantle lid than do models for the Shoal data. This may be due to greater energy loss caused by scattering in the crust along the Bilby profiles. We cannot arrive at firm conclusions with regard to variations of Q with frequency, or its lateral variations, because not only is the scatter in the data relatively large, but also we have no crustal phases that can be used to give an unambiguous Q_e and Q_m model for either of the sets of data.

If lateral variations in Q are present, they are likely to be small. Rather than attempting to force any conclusions regarding lateral changes in Q, we can combine all the data from the four Bilby and Shoal profiles in an attempt to obtain a more reliable average Q model, as well as to obtain more information on the Q variation with frequency. Figure 31 shows all the data out to 1400 km, a range of distance over which we are confident that the P_n arrival is well separated from other phases, with amplitude large enough for a good estimate. We find evidence for a frequency-dependent Q model, with $Q_e(1.25) \approx 1000$, $Q_m(1.25) \approx 400$, and $Q_e(0.875) \approx 1000$, $Q_m(0.875) \approx 300$.

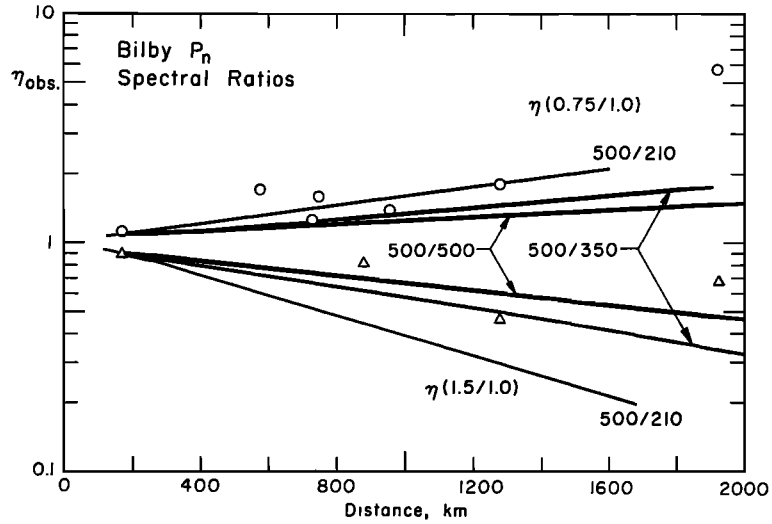

Fig. 30. Observations of the differential attenuation of the P_n spectral ratios from the Bilby explosion in two frequency bands (0.75–1.0 cps and 1.0–1.5 cps). The theoretical curves are computed from the crust and mantle lid Q values indicated. The Q model fitting the data for the 0.75–1.0 cps ratio appears to be quite different than that inferred from the data for the 1.0–1.5 cps ratio and suggests a frequency-dependent Q.

Although the data appear definitely to require different Q models at the two different mean frequencies, the obvious explanation that the intrinsic dissipation is frequency-dependent is not the only one: we could also interpret this as an indication that the attenuation is partly due to the leakage of energy into the low-velocity zone. This effect would be greater for the longer-wavelength (lower frequency) waves, in agreement with the lower Q found at lower frequencies. However, we obtained the Q structure shown in Figure 12 by methods that are not affected by such leakage. The Q structure derived shows larger Q at the short-period body-wave frequencies relative to the Q structure determined from long-period surface waves. Thus both our results are consistent and the only explanation applicable to both and in agreement with all observations is that the intrinsic Q increases with frequency. *Kanamori* [1967*b*] also obtained evidence suggesting frequency-dependent dissipation in the earth. As we have already remarked, this appears to us to be only a very good possibility rather than a demonstrated fact, and more data and a more precise interpretational method will be required before we can draw definite conclusions. Needless to say, a determination of the frequency dependence of the intrinsic dissipation is very important if we hope to use this parameter to estimate material properties and the temperature distribution in the earth.

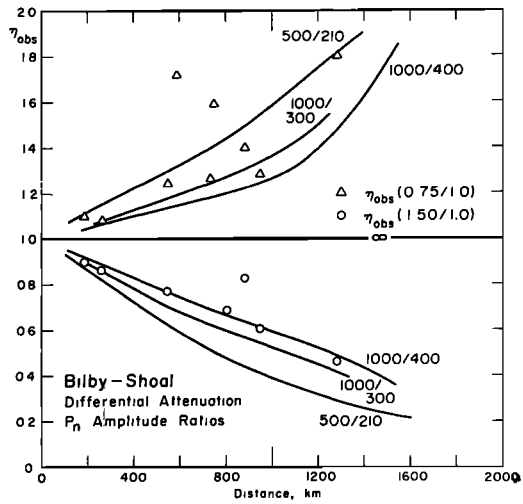

Fig. 31. Differential attenuation data from all profiles combined. The data for the higher-frequency band require Q models with larger values of Q_m and Q_c than do the data in the 0.75- to 1.0-cps band.

Summary and Discussion of Results

We have shown that modern computer-based techniques of processing and analyzing seismic data can be used systematically to isolate and identify mantle body phases in a manner that greatly increases the reliability of the travel-time and amplitude information contained in these phases. Our techniques allow us to obtain reliable data for later arrivals, and we have been able to define the complete travel-time and amplitude-distance curves, rather than just first arrival branches. We therefore have been able to obtain a large amount of information from a relatively small number of observations along a single profile, or linear array. Since we use amplitude data as well as travel-time data, together with constraints supplied by independent observations of travel-time delays and P_n velocities, we conclude that this body of basic data is quite sufficient to define physically meaningful velocity structures.

It should be noted that structures derived from only the first arrivals, or from averages from the arrivals on all branches, show a smooth variation of velocity with depth, cutting right through the upper mantle transition zones obtained in this study. It is not to be expected that meaningful conclusions regarding the composition, structure, and internal state of the earth can be drawn from such models.

We can associate the structures obtained with particular physiographic or geographic regions in a reasonably precise fashion when we consider in detail the spatial sampling characteristics of the various phases used in the inversion. We therefore have been able to obtain regional mantle structures that are correlated with geologic and tectonic characteristics of the appropriate regions. In addition, since we minimize the effects of lateral variations along a given profile by weighting the data according to information supplied by spatial variations of the travel-time delays, P_n velocity variations, and variations in physiography and geology, we obtain velocity-depth variations that are less influenced by lateral variations than is normally the case.

The validity of the structures obtained can be checked in a number of ways. In this study we have pointed out the strong correlations in the amplitude-distance and time-distance curves between profiles. This adds weight to the conjecture that there exist general features common to all structures obtained, in particular the presence and properties of the zones of large velocity gradient at 150-, 400-, and 650-km depths. This correlation is also shown by the radiation patterns obtained for the two explosive sources, from which we deduce that the spatial amplitude variation at various frequencies is that proper to an explosive source when the data are interpreted in terms of the multi-branched amplitude-distance and time-distance curves associated with each of the structures. The structures, of course, individually give the relative P delays proper to the regions with which they are associated, as well as the appropriate P_n velocities, so that their differences as well as their common features are consistent with independent data.

Finally, we note that the fitted structures can be used to compute $dT/d\Delta$, and these predictions can then be compared with existing body-wave apparent velocity data. *Johnson* [1967] gives such data for the western United States, with the region predominantly sampled including the regions studied here. Figure 32 shows Johnson's data along with the theoretical $dT/d\Delta$ generated from the two most different structures obtained in the present study. We observe that the agreement is remarkably good, and that the data are bounded by the theoretical predictions from those two structures. This implies that the scatter in the data could be associated with lateral variations; that is, the scatter could be due to sampling from several mantle provinces. Thus, Johnson's data contain a suggestion of differences in structure similar to those obtained more precisely in the present study. We also note that the scatter diminishes for branches associated with the deeper part of the upper mantle in a manner similar to that predicted by these two mantle structures. The data are also in agreement with the over-all features common to both models, in particular the transition regions at 150, 400, and 650 km. Johnson's fitted model, CIT 204, reflects this fact in that it contains these same features.

Figure 33 shows the predicted $dT/d\Delta$ and the data for the two of our models that are most similar to Johnson's model. The agreement is even better, as would be expected. If the scatter is largely due to sampling from different mantle

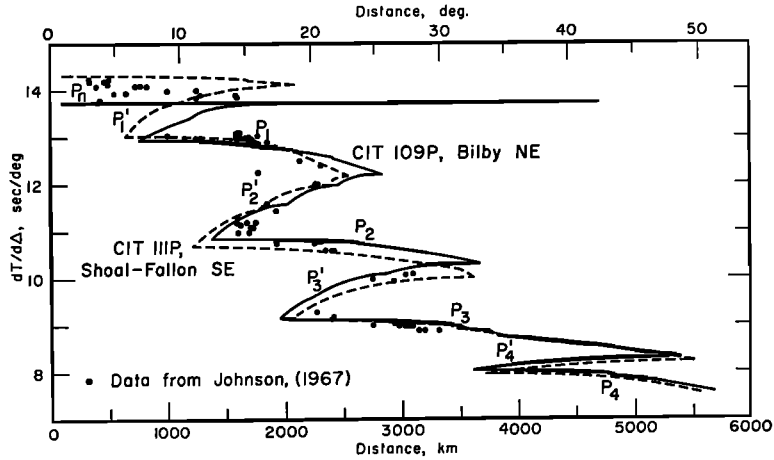

Fig. 32. Comparison of the two most extreme CIT 100 series models with *Johnson's* [1967] $dT/d\Delta$ data from the western United States. The P_n curve for CIT 109P terminates at around 17°. The two velocity structures provide bounds for the $dT/d\Delta$ data for the shallow part of the upper mantle. The data at the greater distances appropriate to the deep upper mantle are in substantial agreement with the predicted variations of both models. The differences beween the predicted curves are indicative of the scatter to be expected in $dT/d\Delta$ data due to lateral variations in the upper mantle velocity structure.

provinces, as our results suggest, then differences between the predicted P_n velocity and a straight line passing through these data are not significant. The greatest discrepancy between the computed and observed $dT/d\Delta$ values in all cases occurs near the cusp formed by the P_2-P_2' branches. This may be due to the fact that the wave form is complicated near the cusp, so that both the $dT/d\Delta$ data and the predictions from the structures we have obtained are more uncertain in these regions. We also observe from our results that the amplitudes along the P_2 and P_2' branches reach maxima at distances beyond the cusp distance, and it is likely that the distribution of Johnson's data reflects this fact as well.

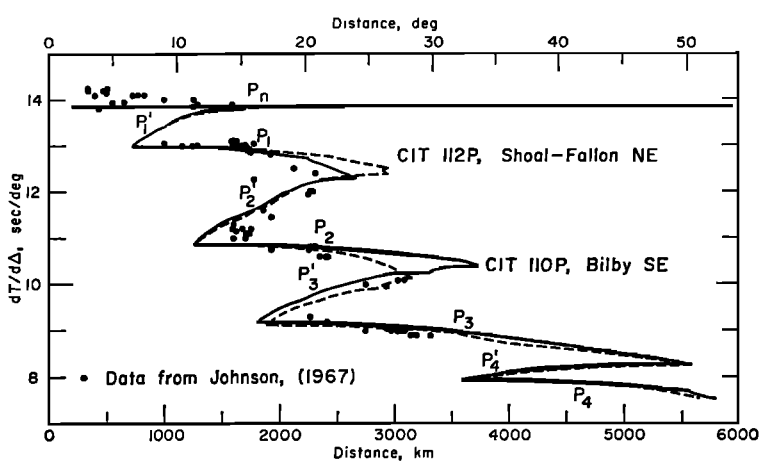

Fig. 33. Comparison of the two models that are most similar to the Johnson CIT 204 mantle model and the $dT/d\Delta$ data. The discrepancy in the predicted and observed $dT/d\Delta$ near the P_2–P_2' cusp is probably due to the fact that the maximum amplitudes are observed to occur near the cluster of $dT/d\Delta$ observations. The curve for P_n terminates at around 17°; the long 'tail' extending beyond 50° is P_1', which has very small energy content.

TABLE 1. Comparison of Mantle Models

CIT 109		CIT 110		CIT 111		CIT 112		CIT 112	
Depth km	V_p	Depth km	V_p	Depth km	V_p	Depth km	V_p	"Midpoint" Depth km	Q
0	6.000	0	6.000	0	6.000	0	6.000	7.0	2000
14.00	6.200	14.00	6.200	14.00	6.200	14.00	6.200	14.05	2000
14.10	6.600	14.10	6.600	14.10	6.600	14.10	6.600	25.55	500
35.00	6.700	37.00	6.700	28.00	6.700	37.00	6.700	37.05	500
35.10	8.048	37.10	7.982	28.10	7.720	37.10	7.980	43.55	500
40.00	8.045	42.00	7.973	45.00	7.719	50.00	7.965	55.00	200
50.00	8.035	50.00	7.966	60.00	7.715	60.00	7 953	65.00	180
60.00	8.020	60.00	7.953	80.00	7.715	70 00	7 935	72.00	180
66.00	8.000	70.00	7.931	90.00	7.719	74.00	7.920	75.50	170
70.00	7.900	80.00	7.700	120.00	7.725	77.00	7.900	77.50	170
74.00	7.840	86.00	7.670	130.00	7.740	78.00	7 860	79.00	160
80.00	7.830	90.00	7.660	140.00	7.800	80.00	7.800	81.00	150
90.00	7.840	100?00	7.685	146.00	7.900	82.00	7.740	84.00	140
100.00	7.870	110.00	7.740	148.00	8.325	86.00	7.700	90.50	140
112.00	7.910	120.00	7.800	170.00	8.335	95.00	7.695	97.50	140
120 00	7.952	130.00	7.888	180.00	8.340	100.00	7.705	105.00	150
130.00	8.015	140 00	8.000	200.00	8.360	110 00	7.748	115.00	160
140.00	8.080	148.00	8.100	250.00	8.435	120.00	7.780	125.00	170
144.00	8.110	151.00	8.200	300.00	8.530	130.00	7.860	133.25	170
148 00	8.160	152.00	8.350	350.00	8.630	136 50	7.910	140.25	180
151.50	8.250	160.00	8.352	375.00	8.730	144.00	8.010	146.50	180
152.00	8.390	170.00	8.354	398.00	9.100	149.00	8.090	150.00	180
160.00	8.390	180 00	8.361	400.00	9.750	151.00	8 170	151.25	200
170.00	8.401	190.00	8.370	450.00	9.800	151.50	8 350	160.75	400
180.00	8.418	200.00	8.379	500.00	9.850	170.00	8.357	175.00	600
200.00	8.429	240.00	8.415	550.00	9.900	180.00	8.362	190.00	800
220.00	8.448	280.00	8.470	600.00	9.950	200.00	8 370	220.00	800
260.00	8.487	337.50	8.560	630.00	10 000	240.00	8.390	260.00	800
355.00	8.617	360.00	8.730	645.00	10.430	280.00	8.420	300.00	800
380.00	8 730	375.00	8.900	660.00	10.930	320.00	8.450	335 00	800
405.00	9.000	381.00	9.000	680.00	10.940	350.00	8.490	362.50	1000
410.00	9.584	384.00	9.100	700.00	10.960	375.00	8.730	382.50	1200
450.00	9.600	388.00	9.600	720.00	10.970	390.00	8.900	394.00	1400
500.00	9.650	450.00	9.635	740.00	11.000	398.00	9.100	398.50	1600
550.00	9.700	500.00	9.660	760.00	11.030	399.00	9.200	399.25	1800
602.00	9.755	550.00	9.686	780 00	11.055	399.50	9.600	424.75	1900
624.00	9.950	580.00	9.713	800.00	11.085	450.00	9.655	475.00	1900
644.00	10.430	605.00	9.800	840.00	11.130	500.00	9.730	525.00	1900
656.00	10.900	619.00	10.050	860.00	11.145	550 00	9.830	575.00	1900
660.00	10.918	630.00	10.390	880.00	11.160	600.00	9.950	605.00	1900
680.00	10.930	635.00	10.893	900.00	11.170	610.00	10.000	620.00	2000
700.00	10.945	680.00	10.927	940.00	11.200	630.00	10 120	635.00	2000
720.00	10.959	700.00	10.942	980.00	11.230	640.00	10.390	647.50	2000
740.00	10.980	717.00	10.955	1054.00	11.280	645.00	10.800	646 25	2000
760.00	11.009	750.00	10.988	1060.00	11.650	647.50	10.950	673.75	2500
780.00	11.034	800.00	11.030	1100.00	11.680	700.00	10.980	720.00	2500
800.00	11.066	840.00	11.060	1200.00	11.800	740 00	11.017	750.00	2500
820.00	11.091	900.00	11.110	1300.00	11.940	760.00	11.046	770.00	2500
840.00	11.111	930.00	11.130	1400.00	12.080	780.00	11.072	790.00	2500
860.00	11.125	980.00	11.163	1500.00	12.210	800.00	11 100	810.00	2500
900.00	11.152	1050 00	11.210	1600.00	12.330	820.00	11.128	830.00	4500
940.00	11.180	1060.00	11.675	1800.00	12.550	840.00	11.148	850.00	4500
980.00	11.207	1100.00	11.695			860.00	11.160	900.00	4500
1030.00	11.240	1200.00	11.760			940.00	11.212	996.50	5500
1036.00	11.610	1300.00	11.870			1053.00	11.275	1056.50	8000
1060.00	11.625	1400.00	12.016			1060.00	11.650	1070.00	8000
1080.00	11.640	1500.00	12.150			1080.00	11.671	1090.00	8000
1100.00	11.665	1600.00	12.280			1100.00	11.690	1150.00	8000
1200.00	11.780	1800.00	12.550			1200.00	11.800	1250.00	8000
1300.00	11.902					1300.00	11.920	1350.00	8000
1400.00	12.016					1400.00	12.016	1450.00	8000
1500.00	12.150					1500.00	12.150	1550.00	8000
1600.00	12.280					1600.00	12.280	1700.00	8000
1800.00	12.550					1800.00	12.550		

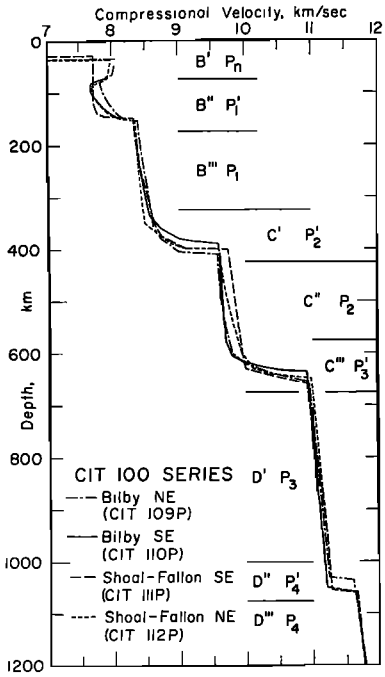

Fig. 34. Upper mantle compressional velocity models for tectonic provinces of the continental United States. The depth zones indicated show the regions sampled by the various phases. The most highly variable regions of the mantle are the B zones sampled by the P_n, P_1, and P_1' phases. Variations between the models in the C and D regions are not considered significant. The transition zones C' and C'''' are well established, but the D'' transition is questionable.

The essential results of this study are the mantle models given in Table 1 and shown in Figure 34. The B zones designated in the figure comprise the depth range within which we are sure that lateral variations in upper mantle properties occur. The C zones appear to be essentially the same for all the models, so that there is probably little lateral variation in this depth range. The C region is a transitional zone for the physical properties of the mantle material and is characterized by two narrow regions of high velocity gradient. Properties of the D zone are less well determined in the present study, but we believe that the D' region of uniform velocity gradient is reliably determined from the combined data from all our profiles. The D'' and D''' regions may be the onset of another transition region in the mantle, but the nature of the transition is certainly not well determined by our data. We conclude, however, that a single change or perhaps several small but rapid changes in velocity gradient do occur in the range from 1000 to 1200 km.

Strong evidence for the existence of the transition zone C'''' has recently been presented by means of seismic data that are completely independent of the material used in the present study. In an earlier study of core phases, Engdahl noticed that in a narrow range of distance on the large-amplitude side of its major caustic, the phase *PKPPKP* was preceded 2½ minutes before the main arrival by a precursor. Subsequent study by *Engdahl and Flinn* [1969] showed that this phase is actually a reflection from a depth of about 650 km, which corresponds to the top edge of the C'''' zone of our models (Figure 34). No reflection was observed from the bottom edge of C'''' or from either edge of C', which implies that the order of the discontinuities at the boundaries of the regions of high velocity gradient is variable. J. H. Whitcomb and D. L. Anderson (personal communication, 1968) have also found a sequence of small reflections from depths less than 900 km. Also, *Adams* [1968] has found precursors to *PKPPKP* which he interprets as reflections from the bottom of the crust and the top of the low-velocity zone.

The existence of a laterally variable zone of low compressional velocity in the upper mantle is a major result of the present study, which has important implications. In particular, the rapid velocity change at both the top and the bottom of the zone, as well as the decrease to low velocity values in between, suggest partial melting of the mantle material in this depth region. *Anderson and Sammis* [1968] have developed this argument in greater detail. We conclude that, although our results strongly imply this interpretation, a conclusive argument depends quite critically on the certainty to be attached to the observed velocity gradients in this region. Although we have made an effort to determine the velocity gradients as accurately as possible for these models by using our amplitude data, we see from the possible variants given for each model that the velocity gradients in this zone nevertheless have a high uncertainty attached to them. The situa-

tion is similar to that described by *Dowling and Nuttli* [1964]. Therefore more data are needed, along with a better method of determining velocity gradients, before we can be more certain of material properties in this region on the basis of seismic observations.

Nevertheless, the partial melting hypothesis is supported by a number of arguments independent of the seismic data [*Mizutani and Kanamori*, 1964; *Spetzler and Anderson*, 1968; *Roy et al.*, 1969; *Anderson and Sammis*, 1968; *Archambeau et al.*, 1968] and is clearly consistent with the models obtained here. It is certainly at least a reasonable working hypothesis. Therefore, if the presence of a low-velocity zone indicates partial melting, we should then expect it to be gravitationally unstable and associated with tectonic activity. The lateral variations in the nature of the low-velocity zone obtained here would therefore, under this hypothesis, imply intense tectonic activity for the Basin and Range province, with less activity (or at least activity of a different kind) in the neighboring plateau and mountain provinces. The low-Q region obtained for the upper mantle suggests partial melting [e.g., *Gordon and Davis*, 1968; *Spetzler and Anderson*, 1968], but again the evidence is not conclusive. The variation of Q with frequency implied by our data is such that a higher Q is observed at higher frequencies. This possibility should be investigated further; if verified, it would be important in determining the mechanism of attenuation and ultimately in determining the physical properties of the material such as the amount of melt component present. However, we need much more reliable information in order to do this.

The transition regions in the C zone are consistent in detail with the solid-solid phase transitions proposed by *Anderson* [1967*b*] and others for the upper mantle and are also consistent with the velocity models obtained from surface waves, which in part motivated the phase transition hypothesis. We consider these particular properties of the upper mantle to be very well established. It remains to establish more fully the D zone transitions and to investigate the possible phase transitions for this temperature and depth range, and, in addition, to investigate further the low-velocity zone and its lateral variability.

Appendix 1. Inversion of Travel Times and Amplitudes

We are concerned with a particular example of nonlinear multivariate analysis. In the usual way [*Anderson*, 1958], the observations are taken to be the sum of, first, a known nonlinear function of known independent variables and of unknown parameters to be estimated and, second, a random error of known or assumed probability distribution. Explicitly, if $T(\mathbf{r}, \boldsymbol{\alpha})$ is the observed quantity and $T_0(\mathbf{r}, \boldsymbol{\alpha})$ the known function of the independent variables $\mathbf{r}$ and unknown parameters $\boldsymbol{\alpha}$, then

$$T(\mathbf{r}, \boldsymbol{\alpha}) = T_0(\mathbf{r}, \boldsymbol{\alpha}) + \epsilon \cdots \tag{A1}$$

states the assumption; in this relation ϵ is a random error. Thus it is assumed that the actual functional $T(\mathbf{r}, \boldsymbol{\alpha})$, in this case the observations, can be approximated by $T_0(\mathbf{r}, \boldsymbol{\alpha})$ with a small random error.

Starting with any convenient first approximation to the unknown vector $\boldsymbol{\alpha}$, we have to first order

$$(T - T_0) = \sum_{k=1}^{N} \left(\frac{\partial T_0}{\partial \alpha_k}\right) \delta\alpha_k + \epsilon \tag{A2}$$

where we have written out the N components of $\boldsymbol{\alpha}$ explicitly. This equation may be regarded as expressing the connection between small variations in T, say $\delta T = T - T_0$, and small variations in $\boldsymbol{\alpha}$, which we denote by $\delta\boldsymbol{\alpha}$. In this context (A2) is rewritten as

$$\delta T = \sum_{k=1}^{N} \left(\frac{\partial T}{\partial \alpha_k}\right) \delta\alpha_k \tag{A3}$$

Thus, we can use (A3) to form a set of linear equations to be solved for the corrections $\delta\boldsymbol{\alpha}$ to the first approximation. Iterations can be made until the $\delta\boldsymbol{\alpha}$ are satisfactorily small.

We need to calculate only the derivatives of T with respect to the $\boldsymbol{\alpha}$ in order to obtain the explicit form of (A3) for travel times. Assuming a radially inhomogeneous earth, with $p = r_p/V_p = dT/d\Delta$ the ray parameter, Δ the surface distance, and r and R radial distances from the earth's center to an arbitrary point and to the earth's surface, respectively, we have [*Bullen*, 1963]

$$T = p\Delta + 2\int_{r_p}^{R} \left[\frac{r^2}{v^2} - p^2\right]^{1/2} \frac{dr}{r}$$

Here r_p and v_p are the radius and velocity at the

point of maximum depth penetration of the ray. We take v to be a function of r and the unknown parameters α, which are to be determined. We can, in straightforward fashion, take derivatives of this integral with respect to α_k, the components of α. We have for this derivative at fixed distance Δ

$$\frac{\partial T}{\partial \alpha_k}_{\Delta} = \frac{\Delta}{v_p}\left[\left(\frac{\partial r_p}{\partial \alpha_k}\right) - \frac{r_p}{v_p}\left(\frac{\partial v_p}{\partial \alpha_k}\right)\right] - 2\left(\frac{r_p}{v_p^2}\right)\left(\frac{\partial r_p}{\partial \alpha_k}\right)\int_{r_p}^{R}\left[\frac{r^2}{v^2} - p^2\right]^{-1/2}\frac{dr}{r} + 2\int_{r_p}^{R}\left[\frac{r^2}{v^2} - p^2\right]^{-1/2} \cdot \left[\frac{r_p^2}{v_p^3}\left(\frac{\partial v_p}{\partial \alpha_k}\right) - \frac{r^2}{v^3}\left(\frac{\partial v}{\partial \alpha_k}\right)\right]\frac{dr}{r}$$

If we use the fact that [*Bullen*, 1963]

$$\Delta = 2p\int_{r_p}^{R}\left[\frac{r^2}{v^2} - p^2\right]^{-1/2}\frac{dr}{r}$$

then we have immediately

$$\left(\frac{\partial T}{\partial \alpha_k}\right)_{\Delta} = -2\int_{r_p}^{R}\left[\frac{1}{v}\left(\frac{\partial v}{\partial \alpha_k}\right)\right] \cdot \left(\frac{r^2}{v^2} - p^2\right)^{-1/2}\frac{r\,dr}{v^2} \qquad \text{(A4)}$$

which is the desired derivative.

Our equations for travel-time inversion by iteration procedures are now of the form

$$\delta T_{\Delta} = \sum_{k=1}^{N}\left(\frac{\partial T}{\partial \alpha_k}\right)_{\Delta}\delta\alpha_k \qquad \text{(A5)}$$

where we propose to compare measured times and calculated times at the same distance. A system of equations is obtained by comparisons at many distances.

We note that the functional dependence of $v(\mathbf{r}, \alpha)$ on α is arbitrary but that we have required v to be a function of radius r only. If $v(r, \alpha_k)$ is taken to be homogeneous in the α_k, for example of the form,

$$v(r, \alpha_k) = \sum_{k=1}^{N}\alpha_k f_k(r)$$

so that for any constant b

$$v(r, b\alpha_k) = bv(r, \alpha_k)$$

then by Euler's theorem

$$\sum_{k=1}^{N}\alpha_k\left(\frac{\partial v}{\partial \alpha_k}\right) = v(r, \alpha_k)$$

Consequently, if we multiply (A4) by α_k and sum over k, we get

$$\sum_{k=1}^{N}\alpha_k\left(\frac{\partial T}{\partial \alpha_k}\right)_{\Delta} = -T \qquad \text{(A6)}$$

where we have used the fact that

$$T = 2\int_{r_p}^{R}\left[\frac{r^2}{v^2} - p^2\right]^{-1/2}\frac{r\,dr}{v}$$

Thus, if $v(r, \alpha_k)$ is homogeneous in the α_k, then so is T. In addition we can calculate the travel time by summing the derivatives.

These relations are precisely what we would get by using Fermats principle and a variational approach. That is, the travel time is given by

$$T = \int_P \frac{ds}{v}$$

with P denoting the ray path. The integral is stationary with respect to small variations in the path. Therefore, the change in T due to variations in v is given by

$$\delta T = -\int_P \left(\frac{\delta v}{v}\right)\frac{ds}{v}$$

If the variations in v are associated with variations in the set of parameters α_k, we get our previous results.

We can of course extend this iteration approach to the amplitudes. If A_p is used to represent the amplitude on a particular branch of the travel-time curve, denoted by an index p, then for fixed p

$$A_p = \left[K_p\frac{d^2T}{d\Delta^2}\right]^{1/2}$$

with K_p considered a fixed function of the velocity at the source and point of observation and with a sign such that the argument of the radical is positive. Employing previous results and methods, we have

$$\frac{\partial A_p}{A_p} = \sum_{k=1}^{N}\left(\frac{\partial \log A_p}{\partial \alpha_k}\right)_{\Delta}\delta\alpha_k \qquad \text{(A7)}$$

where

$$\frac{\partial \log A_p}{\partial \alpha_k} = \frac{1}{2}\frac{d^2}{d\Delta^2}\left(\frac{\partial T}{\partial \alpha_k}\right)_{\Delta}\Big/\frac{d^2T}{d\Delta^2} \qquad \text{(A8)}$$

The derivatives with respect to Δ can be calculated numerically once T and the $(\partial T/\partial \alpha_k)_\Delta$ are determined. Alternatively, we could obtain the partial derivatives analytically from an integral for $d^2T/d\Delta^2$, so that differentiations would not be explicitly involved.

We have supposed a parameterized representation of the velocity function. What we desire is a representation with as few parameters as possible. In this respect, a rational function is quite useful. In this case

$$v(r, \alpha_k) = \sum_{k=0}^{n} a_k r^k \Big/ \sum_{k=0}^{n} b_k r^k \qquad \text{(A9)}$$

Thus, suppose we have a velocity variation with radius at our disposal and we want to generate the appropriate a_k and b_k parameters in a rational function for use in travel-time inversion. If we have $(2n + 1) = N$ values of v versus r, it is easy to show that

$$a_k = d(A_{1,2k+1}) \qquad \text{(A10)}$$

$$b_k = d(A_{1,2k+2})$$

$$k = 0, 1, \cdots, n$$

where $d(A_{i,j})$ is the determinate of the i, j cofactor matrix of a matrix A, which has the form [*Richards*, 1959]

$$A = \begin{bmatrix} 1 & v & r & rv & r^2 & \cdots & r^n & r^n v \\ 1 & v_1 & r_1 & r_1 v_1 & r_1^2 & \cdots & r_1^n & r_1^n v_1 \\ \vdots & & & & & & & \\ 1 & v_{2n+1} & r_{2n+1} & r_{2n+1} v_{2n+1} & r_{2n+1}^2 & \cdots & r_{2n+1}^n & r_{2n+1}^n v_{2n+1} \end{bmatrix} \qquad \text{(A11)}$$

Here v_k and r_k are the discrete points representing the model.

Appendix 2. Tabulated Travel-Time and Amplitude Data

The data have been tabulated by profile, with stations used on more than one profile listed only once.

The 'uncertainty range' tabulated for each arrival represents the time interval in which we estimate that the probability of occurrence of first motion is reasonably large, although not uniform throughout the interval. Outside the interval this probability is small. The following restrictions apply to this definition:

1. In general, the most probable time of arrival is near the earliest possible arrival time. This is in particular true for second arrivals.

2. The uncertainty range for a given phase is used to enclose a time interval in which one or more phases may arrive in some cases. Thus the interval enclosing one phase may be extended when it is felt that two or more phases are arriving although it is only possible to be sure that at least one signal arrives. In this case the probability of the signal's arriving within the interval is not uniform, and so there would be two or more peaks.

3. Two or more observed phases at the same station may be a part of a single phase when the range of uncertainty in their arrival times overlap. This applies to several of the observations near cusps in the travel-time curves.

(The tabular material is available in the microfiche version of this paper.)

Acknowledgments. It is a pleasure to acknowledge the generous cooperation of John Lambert. who ably oversaw the digital data processing, and Bruce Julian, who freely made available to us his program for body-wave calculations, which we modified and used in our work. We also wish to thank our colleagues at the Seismic Data Laboratory and the Seismological Laboratory with whom we have had many beneficial discussions, and whose criticisms have sharpened our arguments in favor of the interpretations in this paper. We thank Bruce Julian, Don Anderson, and R. D. Adams for making available to us their most recent papers in advance of publication.

This research was supported by the Air Force Office of Scientific Research, Office of Aerospace Research, United States Air Force, under AFSOR contracts AF-49(638)-1337 and AF 49(638)-1117 and by the Advanced Research Projects Agency, Nuclear Test Detection Office, Technical Applications Center Contract AF 33(657)-12447.

References

Adams, R. D., Early reflections of *P'P'* as an indication of upper mantle, *Bull. Seismol. Soc. Amer., 58,* 1933, 1968.

Akimoto, S., and H. Fujisawa, Olivine-spinel solid

solution equilibria in the system Mg_2SiO_4-Fe_2SiO_4, *J. Geophys. Res., 73,* 1467–1479, 1968.

Anderson, D. L., Latest information from seismic observations, chap. XII, in *The Earth's Mantle,* edited by T. F. Gaskell, pp. 355–420, Academic Press, London, 1967*a*.

Anderson, D. L., Phase changes in the upper mantle, *Science, 157,* 1165–1173, 1967*b*.

Anderson, D. L., and C. B. Archambeau, The anelasticity of the earth, *J. Geophys. Res., 69,* 2071–2084, 1964.

Anderson, D. L., A. Ben-Menahem, and C. B. Archambeau, Attenuation of seismic energy in the upper mantle, *J. Geophys. Res., 70,* 1441–1448, 1965.

Anderson, D. L., and C. Sammis, The low velocity zone, paper in preparation, 1968.

Anderson, T. W., *An Introduction to Multivariate Statistical Analysis,* John Wiley, New York, 1958.

Archambeau, C. B., Automated inversion of seismic field amplitude—time properties for crust and upper mantle structure (abstract), *Geophys. J., 11,* 254, 1966.

Archambeau, C. B., J. C. Bradford, P. W. Broome, W. C. Dean, E. A. Flinn, and R. L. Sax, Data processing techniques for the detection and interpretation of teleseismic signals, *Proc. IEEE, 53*(12), 1860–1884, 1965.

Archambeau, C. B., and E. A. Flinn, Perturbation theory for the inversion of body wave traveltime data, *Tech. Rep. to U.S. Air Force Tech. Appl. Center (Contract AF 33(657)-15919, SDL Rep. 142),* Earth Sciences Division, Teledyne Industries, Inc., 1966.

Archambeau, C. B., E. A. Flinn, and D. G. Lambert, Detection, analysis, and interpretation of teleseismic signals, 1, *J. Geophys. Res., 71,* 3483–3501, 1966.

Archambeau, C. B., E. A. Flinn, and D. G. Lambert, Detection, analysis, and interpretation of teleseismic signals, 2 (abstract), *Geophys. J., 13,* p. 369, 1967.

Archambeau, C. B., R. Roy, D. Blackwell, D. L. Anderson, L. Johnson, and B. Julian, A geophysical study of continental structure (abstract), *Trans. Amer. Geophys. Union, 49,* 328, 1968.

Barr, K. G., Upper mantle structure in Canada from seismic observations using chemical explosions, *Can. J. Earth Sci., 4,* 961–975, 1967.

Berry, M. J., and C. F. West, Reflection and head wave amplitudes in a medium of several layers, in *The Earth beneath the Continents, Geophys. Monogr. 10,* edited by J. S. Steinhart, and T. J. Smith, pp. 464–481, American Geophysical Union, Washington, D. C., 1966.

Brune, J. N., Surface waves and crustal structure, in *The Earth's Crust and Upper Mantle, Geophys. Monogr. 13,* American Geophysical Union, Washington, D. C., in press, 1969.

Brune, J. N., and J. Dorman, Seismic waves and earth structure in the Canadian shield, *Bull. Seismol. Soc. Amer., 53,* 167–209, 1963.

Bullen, K. E., *Introduction to the Theory of Seismology,* 3rd ed., Cambridge University Press, New York, 1963.

Caner, B., W. H. Cannon, and C. E. Livingstone, Geomagnetic depth sounding and upper mantle structure in the Cordillera region of western North America, *J. Geophys. Res., 72,* 6335–6351, 1967.

Cleary, J. R., and A. L. Hales, An analysis of the travel times of *P* waves to North American stations, in the distance range 32° to 100°, *Bull. Seismol. Soc. Amer., 56,* 462–489, 1966.

Dowling, J. J., and O. W. Nuttli, Travel-time curves for a low-velocity channel in the upper mantle, *Bull. Seismol. Soc. Amer., 54,* 1981, 1964.

Engdahl, E. R., and E. A. Flinn, Seismic waves reflected from discontinuities within earth's upper mantle, *Science, 163,* 117, 1969.

Fujisawa, H., Temperature and discontinuities in the transition layer within the earth's mantle: Geophysical application of the olivine-spinel transition in the Mg_2SiO_4-Fe_2SiO_4 system, *J. Geophys. Res., 73,* 3281–3294, 1968.

Gordon, R. B., and L. A. Davis, Velocity and attenuation of seismic waves in imperfectly elastic rock, *J. Geophys. Res., 73,* 3917–3935, 1968.

Gordon, R. B., and C. W. Nelson, Anelastic properties of the earth, *Rev. Geophys., 4,* 457–474, 1966.

Green, R. W. E., and A. L. Hales, The travel times of *P* waves to 30° in the central United States and upper mantle structure, *Bull. Seismol. Soc. Amer., 58,* 267, 1968.

Hales, A. L., J. R. Cleary, H. A. Doyle, R. Green and J. Roberts, P-Wave Station Anomalies and the Structure of the Upper Mantle, *J. Geophys. Res., 73,* 3885–3896, 1968.

Herrin, E., and J. Taggart, Regional variations in P_n velocity and their effect on the location of epicenters, *Bull. Seismol. Soc. Amer., 52,* 1037–1046, 1962.

Isacks, B., J. Oliver and L. Sykes, Seismology and the New Global Tectonics, *J. Geophys. Res., 73,* 5855–5900, 1968.

Jackson, D., and D. L. Anderson, Physical mechanisms of seismic wave attentuation, to appear, *Rev. Geophys., 8*(1), 1970.

Johnson, L. R., Array measurements of *P* velocities in the upper mantle, *J. Geophys. Res., 72,* 6309–6325, 1967.

Julian, B. R., and D. L. Anderson, Travel times, apparent velocities, and amplitudes of body waves, *Bull. Seismol. Soc. Amer., 58,* 339–366, 1968.

Kanamori, H., Upper mantle structure from apparent velocities of *P* waves recorded at Wakayoma Micro-Earthquake Observatory,

Bull. Earthquake Res. Inst., Tokyo Univ., 45, 657–678, 1967*a*.

Kanamori, H., Attenuation of *P* waves in the upper and lower mantle, *Bull. Earthquake Res. Inst. Tokyo Univ., 45,* 299–312, 1967*b*.

Karal, F. C., Jr., and J. B. Keller, Elastic wave propagation in homogeneous and inhomogeneous media, *J. Acoust. Soc. Amer., 31,* 694–705, 1959.

Lewis, B. T. R., and R. B. Meyer, A seismic investigation of the upper mantle to the west of Lake Superior, *Bull. Seismol. Soc. Amer., 58,* 565–596, 1968.

Mizutani, H., and H. Kanamori, Variation of elastic wave velocities and attenuation property near the melting temperature, *J. Phys. Earth, 12,* 43, 1964.

Niazi, M., and D. L. Anderson, Upper mantle structure of western North America from apparent velocities of *P* waves, *J. Geophys. Res., 70,* 4633–4640, 1965.

Pakiser, L. C., and R. Robinson, Composition of the continental crust as estimated from seismic observations, in *The Earth beneath the Continents, Geophys. Monogr. 10,* edited by J. S. Steinhart and T. J. Smith, pp. 620–626, American Geophysical Union, Washington, D. C., 1966.

Richards, P. E., *Manual of Mathematical Physics,* p. 257, Pergamon Press, New York, 1959.

Roy, R. F., D. D. Blackwell, and F. Birch, Heat generation of plutonic rocks and continental heat-flow provinces, *Earth Planet. Sci. Lett., 5,* 1–12, 1968.

Spetzler, H., and D. L. Anderson, The effect of temperature and partial melting on velocity and attenuation in a simple binary system, *J. Geophys. Res., 13,* 6051–6060, 1968.

Steinhart, J. S., and R. P. Meyer, Explosion studies of continental structure, *Carnegie Inst. Wash. Publ. 622,* 409 pp., 1961.

Toksöz, M. N., and D. L. Anderson, Phase velocities of long-period surface waves and structure of the upper mantle, 1, Great-circle Love and Rayleigh wave data, *J. Geophys. Res., 71,* 1649–1658, 1966.

Vine, F. J., and D. H. Matthews, Magnetic anomalies over ocean ridges, *Nature, 199,* 947–949, 1963.

Willden, R., Seismic refraction measurements of crustal structure between American Falls Reservoir, Idaho, and Flaming George Reservoir, Utah, *U. S. Geol. Surv. Prof. Pap. 525-C,* C44-C50, 1965.

Woollard, G. P., Regional isostatic relations in the United States, in *The Earth beneath the Continents, Geophys. Monogr. 10,* edited by J. S. Steinhart and T. J. Smith, pp. 557–594, American Geophysical Union, Washington, D. C., 1966.

(Received March 3, 1969;
revised July 18, 1969.)